

*Biochemistry*. Author manuscript; available in PMC 2008 October 13.

Published in final edited form as:

Biochemistry. 2006 March 28; 45(12): 3875–3886. doi:10.1021/bi0523097.

Characterization of the spontaneous "aging" of the heme oxygenase from the pathological bacterium *Neisseria meningitidis* via cleavage of the C-terminus in contact with the substrate; Implications for functional studies and the crystal structure<sup>†</sup>

Yangzhong Liu $^{\ddagger}$ , Li-Hua Ma $^{\ddagger}$ , Xuhong Zhang $^{\S}$ , Tadashi Yoshida $^{\S}$ , James D. Satterlee $^{\perp}$ , and Gerd N. La Mar $^{\ddagger,*}$ 

‡Department of Chemistry, University of California, Davis, CA 95616

§Department of Biochemistry, Yamagata University School of Medicine, Yamagata 990-9585, Japan

⊥Department of Chemistry, Washington State University, Pullman, WA 99164

### **Abstract**

Solution <sup>1</sup>H NMR spectroscopy and mass spectrometry are utilized to characterize the irreversible "aging" of native heme oxygenase from N. meningitidis, NmHO. 2D NMR characterization of the cyanide-inhibited substrate complex shows that the C-terminal interaction between Arg208His209 and the exposed pyrrole of the protohemin substrate in the "native" NmHO complex is lost in the "aging". Mass spectrometry and N-terminal sequencing of WT and "aged" NmHO reveal that the "aging" process involves cleavage of the Arg208His209 dipeptide. The construction of the double deletion mutant without Arg208His209 and its NMR comparison as both the resting state substrate complex and its cyanide-inhibited complex with the "aged" NmHO reveals that cleavage of the Cterminal dipeptide is the only modification during the aging. Comparison of cyanide ligand binding constants reveal a factor ~1.7 greater CN<sup>-</sup> affinity in the native vs "aged" NmHO. The rate of protohemin degradation and its stereoselectivity are unaffected by the C-terminal truncation. However, the free  $\alpha$ -biliverdin yield in the presence of desferrioxamine is significantly increased in the "aged" NmHO and its deletion mutant relative to WT, arguing for a role of the NmHO C-terminus in modulating product release. The facile cleavage of Arg208His209 in the resting state complex, with half-life of ~24h at 25°C, suggests that previous characterization of NmHO may have been carried out on mixture of native and "aged" NmHO, and may account for the "lost" C-terminal residues in the crystal structures.

### INTRODUCTION

The pathological bacterium *Neisseria meningitidis* utilizes a heme oxygenase, HO (named *Nm*HO, also HemO (1)), for securing the iron needed for host infection. Similarly sized, soluble HOs (~210 residues) have been identified in numerous other bacteria, including those from *C. diphtheriae* (*Cd*HO) (2) and *P. aeruginosa* (*Pa*HO) (3). The bacterial HOs exhibit variable

<sup>&</sup>lt;sup>†</sup>This work was supported, in part, by the National Institutes of Health, GM62830 (GNL) and a grant-in-Aid for Scientific Research (16570102) for the Minority of Education and Sports, Science and Teaching, Japan (T.Y.)

<sup>\*</sup>Corresponding author: Gerd N. La Mar, Department of Chemistry, University of California, Davis, One Shields Avenue, Davis, CA 95616, Phone: (530) 752-0958, FAX: (530) 752-8995, e-mail: lamar@chem.davis.edu.

sequence homology among themselves and with the more extensive studied mammalian HOs. (4-6) The latter HOs are larger ( $\sim$ 300 residues) and membrane-bound, but expression of truncated, soluble constructs where the C-terminal membrane anchor helix is deleted, (7-9) yields soluble HOs with conserved activity. The various HOs appear to share a common mechanism, worked out for human (hHO) and rat (rHO) enzymes,(4,5,9-12) where the reactive ferric hydroperoxy (13) species stereoselectively hydroxylates one protohemin (PH:Figure 1) meso-position, which, with sequential  $O_2$  and electrons, forms verdoheme and ferric-biliverdin as degradation intermediates (Scheme 1). Reduction of the iron in the latter intermediate results in loss of iron, followed by slow ( $\sim$ 0.03 s<sup>-1</sup>) dissociation of the product biliverdin.(9) In mammals, this very slow dissociation step is strongly accelerated by forming a transient 1:1 complex with biliverdin reductase, BVR, with the BVR:HO contact near the exposed pyrrole of the substrate/product. (14)

The physiologically relevant, ferrous HO-substrate complex of O<sub>2</sub> or the ferric hydroperoxy species are, with one notable exception (15), insufficiently stable for detailed crystallographic or solution NMR structural studies. This has necessitated the use of the ferrous NO and CO, or ferric CN<sup>-</sup>, N<sub>3</sub><sup>-</sup> or OH<sup>-</sup> derivatives as model complexes. Crystal structures of both mammalian (16-19) and bacterial (15,20-24) HO-PH complexes reveal a common fold, in spite of their variation in sequence, with a mobile distal helix placed close to the substrate protohemin, PH (Figure 1), so as to block all but one of the four meso positions to electrophilic attack by the hydroperoxide. (9,12) The distal helix backbone sterically orients all axial ligands (and presumably the hydroperoxide), toward the sole "open" meso position. A series of distal ordered water molecules were also detected (15,17,18,20-23,25) in all HO complexes and proposed to stabilize the unusual hydroperoxy complex. (12) The common seating of PH in HOs leads to unique  $\alpha$ -meso cleavage(9) in all but PaHO, (23,26) where a 90° in-plane rotation of PH relative to PH in other HOs, leads primarily to δ-meso cleavage. Solution NMR studies have shown that common heme orientational isomerism about the  $\alpha$ -, $\gamma$ -meso axis, (27-30) as well as more novel, dynamic, in-plane rotational isomerism, (26,31,32) are natural characteristics of HO-substrate complexes and that the ordered distal water molecules (29, 30,33,34) are embedded in an extended H-bond network that involves some remarkably strong H-bonds.

None of the crystal structures of HOs have detected (15,17,18,20-23,25) the N- and C-terminal residues, with these "missing" residues attributed to disorder, as is common to the majority of crystal structures. In the case of *Nm*HO however, it was noted (20,21) that the "missing" C-terminal residues could be placed closer to the substrate binding site than in other HOs. Solution <sup>1</sup>H NMR studies of the cyanide-ligated substrate complex of *Nm*HO have confirmed (30) a conserved molecular structure relative to that in crystals,(20) with several residues, and one PH propionate, exhibiting alternate orientations depending on whether a H-bond donor (20) (H<sub>2</sub>O) or an H-bond acceptor (21) (NO, CN<sup>-</sup>) is ligated to the iron. A notable difference between the *Nm*HO-PH-CN solution structure (30) and either the *Nm*HO-PH-H<sub>2</sub>O or *Nm*HO-PH-NO crystal structures (20,21) is that the former detects a direct interaction between one of the C-terminal His and pyrrole D (Figure 1) of the PH substrate. A simple model suggested (30) that Arg208 forms a salt bridge with the 7-propionate of the heme, with the His ring possibly H-bonding the Asp27 carboxylate. While the C-terminus clearly interacts with substrate in solution, the details as to which C-terminal His (207 or 209) interacts with the heme, as well as the nature of this interaction, are not yet clear.

We noted earlier (30) that, in solution, the initially prepared NmHO-PH-CN or NmHO-PH-H<sub>2</sub>O, described as the 'A' form, spontaneously, homogeneously, but irreversibly, convert into another species, referred to the 'X' form, with altered heme hyperfine shifts in substrate complexes. Our interest here is to characterize the nature of the structural change that accompanies this 'A' $\rightarrow$ 'X' transition due to "aging" in the physiologically relevant, resting

state, high-spin ferric complex, *Nm*HO-PH-H<sub>2</sub>O. However, strong relaxation obscures the majority of the key active site residues of interest in this complex, although even the simple spectrum of this complex allows detection of the formation of 'X' (see below). Hence, we will structurally characterize the "aged" complex trapped as the low-spin, cyanide-inhibited complex, *Nm*HO-PH-CN, which provides the narrow NMR lines needed for definitive assignment and structural characterization and exhibits hyperfine shifts readily interpreted in terms of details of the active site molecular structure.(30,33,35) <sup>1</sup>H NMR assignment of the majority of the relevant active site residues for the 'A' form of *Nm*HO-PH-CN has been reported.(30)

In this study, we revisit this 'A'  $\rightarrow$  'X' conversion to characterize by <sup>1</sup>H NMR the nature of the structural change that accompanies this conversion and to assess the relationship of this conversion to the interaction between the C-terminus and the substrate. We rely on <sup>1</sup>H NMR to demonstrate that the 'A' -- 'X' conversion results in the loss of the C-terminal interaction with the substrate, and we rely on mass spectrometry to demonstrate that the 'A' - 'X' conversion entails a cleavage of the C-terminal Arg208 and His209 residues. We further show that this loss of the C-terminal interaction with substrate results in perturbed ligand affinity for the substrate iron and product biliverdin release, arguing for a functional role of the C-terminus in modulating heme reactivity. The detailed mechanism of the peptide cleavage in the NmHO 'A'  $\rightarrow$  'X' conversion is yet to be determined, but a half-life of as short as 1 day for the 'A' → 'X' conversion is observed. Hence the facility of this 'A'- 'X' conversion for NmHO suggests the possibility that structural and functional characterization for NmHO and its substrate complexes may have been, or are being, performed on variable mixtures of the 'A' and 'X' form, or possibly, on primarily the 'X' form. We emphasize here the elucidation of the structural difference in the 'A' vs 'X' species and identify a simple analytic marker for species 'X'.

# **Experimental Procedures**

### **Protein preparation**

The WT apo NmHO samples utilized in this study are the same as those described in detail previously. (30) All samples were kept frozen at -80°C until required. Stoichiometric amounts of hemins were added to apo NmHO in phosphate buffer (100 mM or 50 mM, pH 7.0). The substrate complex was purified by column chromatography on Sephadex G25 and concentrated to 1-3 mM by ultrafiltration. KCN buffered at pH 7.0 was added in ~10 fold excess to prepare the cyanide complex, NmHO-PH-CN.  $^2$ H<sub>2</sub>O for  $^1$ H<sub>2</sub>O solvent exchange was carried out by column chromatography.(36)

The plasmid for the two C-terminal residue deletion mutant, named  $\Delta$ C2-NmHO, with Arg208 and His209 absent, was constructed as follows. PCR was carried out with an NmHO expression vector, NmHO (30) (formerly pMWHemO), as a template and a synthetic nucleotide F and  $\Delta$ C2R as primers. The nucleotide F (5'-AATACGACTCACTATAGGGAGACCACAAC-3') corresponds to the nucleotide sequence positions form -79 to -51 of pMW172, and the nucleotide  $\Delta$ C2R (3'-

GGCCTTCCTTACTACGGCGTGATCGTGATTCGAATCCGGTGTTCA-5') corresponds to the complementary nucleotide sequence positions from 607 to 644 of pMWNmHO, except that 3'-TCC-5' codon for Arg208 was changed to 3'-ATC-5' to create a stop codon. The second A in the NdeI recognition site, CATATG, is defined as +1. The target fragment was cut with NdeI and HindIII, and ligated into pMW172 to construct pMWNmHO $\Delta$ C2. Expression and purification of the  $\Delta$ C2-NmHO mutant were similar to those described for wild-type enzyme.

Samples of WT *Nm*HO-PH-H<sub>2</sub>O were "aged" in <sup>1</sup>H<sub>2</sub>O solution, 50 mM in phosphate, and pH 7.0 at 25°C for 5-160 hr. The "aging" was monitored by mass spectrometry and <sup>1</sup>H NMR as

either the NmHO-PH-H<sub>2</sub>O or, for structural characterization, the cyanide-trapped NmHO-PH-CN complex. The influences of O<sub>2</sub> and a general protease inhibitor cocktail (Sigma Chemicals; catalog No. P2714) on 'A' to 'X' conversion were assessed by careful exclusion of O<sub>2</sub> in sample preparation and by adding 0.1  $\mu$ m of the inhibitor cocktail in 4 hr intervals to a split sample of NmHO<sup>A</sup>-PH-H<sub>2</sub>O, where the second portion served as control.

### **NMR** spectroscopy

<sup>1</sup>H NMR data were collected on Bruker AVANCE 500 and 600 spectrometers operating at 500 and 600 MHz, respectively. Reference spectra were collected in both <sup>1</sup>H<sub>2</sub>O and <sup>2</sup>H<sub>2</sub>O over the temperature range 15-35°C at a repetition rate of 1 s<sup>-1</sup> using a standard one-pulse sequence. Chemical shifts are referenced to 2,2-dimethyl-2-silapentane-5-sulfonate (DSS) through the water resonance calibrated at each temperature. 600 MHz NOESY (37) spectra (mixing time, 40 ms; 15-35°C) using both hard pulse and "3:9:19" detection (38) and 500 MHz Clean-TOCSY (to suppress ROESY response (39)) spectra (25°, 35°C, spin lock 25 and 40 ms) using MLEV-17 (40) were recorded over a bandwidth of 25 KHz (NOESY) and 12 KHz (TOCSY) with recycle times of 500 ms and 1s, using 512 t1 blocks of 256 scans each consisting of 2048 t2 points. 2D data sets were processed using Bruker XWIN software on a Silicon Graphics Indigo workstation and consisted of 30°- or 45°-sine-squared-bell-apodization in both dimensions, and zero-filling to 2048 × 2048 data points prior to Fourier transformation.

Simple molecular modeling of the C-terminus was carried out by the standard program in the Accelerys Insight package, using the X-ray coordinates (21) (PDB access 1J77) of residues 8-206 and the His207 peptide NH H-bond to the Asp27 carboxylate and the Arg208 guanidyl H-bond to the 7-propionate carboxylate as constraints.

### Mass spectrometry

Matrix Assisted Laser Desorption Ionization-Time of Flight (MALDI-TOF) mass spectrometry was carried out on a Voyager DE system (Perseptive Biosystems) housed in the Washington State University Laboratory for Biotechnology and Bioanalysis, Unit 2 (WSU LBB2). Five primary matrix solutions were employed in replicates of each NmHO sample. These were made from saturated solutions of Sinapinic Acid (3,5-dimethoxy-4-hydroxycinnamic acid, Aldrich or Sigma). The aqueous solutions used to dissolve the matrix were: (i) 30%-0.1% trifluoroacetic acid/70% acetonitrile (Sigma) by volume; (ii) 30%-1.0% trifluoroacetic acid/70% acetonitrile; (iii) 50%-1.0% trifluoroacetic acid/50% acetonitrile; (iv) 30%-1.0% acetic acid/70% acetonitrile; (v) 50%-1.0% acetic acid/50% acetonitrile. Protein samples (1 µL) were thoroughly pipette mixed with an equal volume of the matrix solution on the MALDI-TOF plate until crystallization began. For calibration purposes, standard desalted solutions of (all from Sigma) equine myoglobin ( $M_r$ =16,952.56) and equine cytochrome c(M<sub>r</sub>=12,361.14) were incorporated in some solutions as internal standards for accurate mass/ charge determinations. Mass statistics were accumulated using repeated mass determinations in separate MALDI-TOF experiments with at least two internal references present. Individual protein masses were calculated using the averaged isotope masses of each element (IUPAC Commission on Atomic Weights and Isotopic Abundances, 1993): H=1.00794, C=12.011, N= 14.00674, O=15.9994, S=32.066. Protein masses were then constructed from the calculated mass of each amino acid and the specific primary amino acid sequence. The values reported are further rounded to units place.

## N-terminal sequencing

Amino-terminal protein sequencing (up to 12 amino acids) was carried out in the Washington State University Laboratory for Biotechnology and Bioanalysis, Unit 1 (WSU LBB1) using an Applied Biosystems Procise 492 Protein Sequencer.

### NmHO activity

Optical absorption spectra were recorded on a Beckmann, DU 7400 spectrophotometer at  $30^{\circ}$  C between 250 and 750 Nm. Standard reaction mixture consists of  $10 \,\mu\text{M} \,Nm\text{HO-PH-H}_2\text{O}$  complex in  $1.5 \,\mu\text{l}$  of 50 mM phosphate (pH 7.4). After 3 min pre-incubation, the reaction was started by the addition of 15 ml of 1 M sodium ascorbate (final concentration,  $10 \,\text{mM}$ ). When desferrioxamine was added, a final concentration of 1 mM was used. Stereoselectivity of the reaction products was analyzed by HPLC (41) after being hydrolyzed with HCl to ensure the full conversion into biliverdin.

## **RESULTS**

### Effect of the 'A'→'X' conversion on NMR spectra

The expected (16,20) and observed,(30) dipolar contacts between protohemin and active site residues, and among active site residues, in WT NmHO-PH-CN, are shown schematically in Figure 1. The unexpected contacts of His207 and Arg208 (each shown in bold) with pyrrole D observed (30) in NmHO<sup>A</sup>-PH-CN (and lost in NmHO<sup>X</sup>-PH-CN; see below), are shown by dashed lines. The resolved portions of the 500 MHz  $^1$ H NMR spectrum of native or 'A' highspin NmHO<sup>A</sup>-PH-H<sub>2</sub>O complex are illustrated in Figure 2A, where we provide the previously determined (42) heme methyl, vinyl  $H_b$  and axial His  $C_b$ H assignments. Figure 2B represents the  $^1$ H NMR spectrum of a NmHO-PH-H<sub>2</sub>O sample "aged" ~24 h at 25°C that contains ~45% NmHO<sup>A</sup>-PH-H<sub>2</sub>O and ~55% NmHO<sup>X</sup>-PH-H<sub>2</sub>O, and Figure 2C represents the spectrum of a NmHO-PH-H<sub>2</sub>O sample aged for a week at 25°C, which corresponds to >95% NmHO<sup>X</sup>-PH-H<sub>2</sub>O. It is noted that in the high-spin, resting state complex reference NMR spectrum, only the 8CH<sub>3</sub> "senses" the structural difference between the 'A' and 'X' complexes (in 2D, the NmHO-PH-H<sub>2</sub>O Asp24  $C_\beta$ Hs reveal altered chemical shifts, not shown; see Supporting Information). Moreover, some ~10% of 'X' is already present in the initial complex in Figure 2A, as shown by the low-field shoulder to the 8CH<sub>3</sub> peak.

The resolved portions of the 600 MHz  $^{1}$ H NMR spectrum of the wild-type, enzyme as the *Nm*HO-PH-CN complex are displayed in Figure 3A. The major component (>90% and labeled species 'A') represents the equilibrium, native complex, as also shown in Figure 2A, (peaks with superscript A) with the PH orientation as described in the both crystal (16, 30) and solution structures, and shown in Figure 1. The resonance assignments are those described in detail previously(30) for the PH orientation shown in Figure 1. Heme methyls for two minor components are also observed in Figure 3A. The peak labeled  $^{3}$ CH<sub>3</sub>B arises from the native *Nm*HO-PH-CN with PH rotated 180° about the  $\alpha$ - $\gamma$ -meso axis (species 'B'). The 'B' and 'A' species are comparably populated immediately after assembling the complex in solution, but rapidly equilibrate to a 10:1 'A':'B' ratio,(30) as shown in Figure 3A. A third (~5%) species, (30) which we designated 'X', gives rise to methyl peak labeled  $^{3}$ CH<sub>3</sub>X, is variably present upon preparing the complex under a variety of conditions and corresponds to the species in Figure 3C. No further  $^{1}$ H NMR changes are observed over several months after conversion to 'X' as either the *Nm*HO<sup>X</sup>-PH-H<sub>2</sub>O or *Nm*HO<sup>X</sup>-PH-CN complexes.

The 'A' → 'X' conversion in the NmHO-PH-H<sub>2</sub>O complex has a half-life of ~24 h at 25°C in the presence of ~50 mM phosphate at pH 7.2. Interconversions among the "aged" NmHO-PH-H<sub>2</sub>O and NmHO-PH-CN complexes reveals that the same species X is formed in the two derivatives (data not shown). The 'A' → 'X' half-life is significantly reduced by replacing the PH vinyls with methyls (Liu, Yoshida, La Mar, unpublished observations). Exclusion of O<sub>2</sub> from a sample had no detectable effect on the conversion rate for the NmHO<sup>A</sup>-PH-H<sub>2</sub>O complex. Addition of cyanide slowed the 'A' → 'X' rate significantly for each hemin, but even the cyanide complex eventually converted to the 'X' complex at a rate much faster upon replacing vinyls with methyls. Lastly, the introduction of a bacterial protease inhibitor cocktail

failed to have a detectable effect on the rate of 'A'—'X' conversion (NMR data shown in Supporting Information). Hence co-purified *E. coli* proteases are not likely the cause of the 'A'—'X' conversion. Clearly more extensive studies well outside the scope of this report are needed to elucidate this mechanism.

## Structural characterization of the heme cavity for NmHOX-PH-CN

The hyperfine shift pattern for resolved resonances is very similar for *Nm*HO<sup>A</sup>-PH-CN and *Nm*HO<sup>X</sup>-PH-CN (compare Figures 3A and 3C), so that the same 2D <sup>1</sup>H NMR approaches reported in detail for the former complex,(30) yield similarly complete assignment for the latter complex. Hence only very limited 2D data are provided that display *differences* in the two complexes. Additional 2D data for *Nm*HO<sup>X</sup>-PH-CN are provided in Supporting Information. The chemical shifts for the heme and the most strongly hyperfine-shifted residues in the two complexes are compared in Table 1, with the data for the remainder of the 55 assigned residues provided in Supporting Information. Except for primarily the heme 8CH<sub>3</sub> and more weakly, the heme 1CH<sub>3</sub> (see below), very similar NOESY cross peak patterns between heme and residues, and among residues, are observed in the 'A' and 'X' *Nm*HO-PH-CN complexes.

The key differences in heme contacts between the 'A' and 'X' species are illustrated in the portions of the NOESY spectra involving the heme 8CH<sub>3</sub> and 1CH<sub>3</sub> peaks, as illustrated in Figure 4 for  $NmHO^A$ -PH-CN (Figures 4A-4I) and  $NmHO^X$ -PH-CN (Figures 4A', 4H'; and 4I'), complexes. The crystal structures of NmHO complexes predict(16,21) 8CH<sub>3</sub> NOESY cross peaks only to Gly120  $C_\alpha H$  (under  $7H_\alpha$  in Figs. 4A, 4B, but resolved at other temperatures). However, the actual NOESY spectra exhibit many more cross peaks. For  $NmHO^A$ -PH-CN (Figures 4A, 4B, 4C), a TOCSY-detected His ring (labeled His I), the  $C_\beta Hs$  of the TOCSY-detected NH- $C_\alpha H$ - $C_\beta H_2$  backbone of His I (His207) (Figure 4C), as well as the obvious  $C_\alpha H$  of another residue exhibit significant intensity NOESY cross peaks to the 8-CH<sub>3</sub>. Since the  $C_\alpha H$  peak at 3.84 ppm exhibits no common NOESY cross peak to the rings of either His207 or His209 (see below), it can be assigned to the only other possible residue, Arg208. One of the His I  $C_\beta Hs$  exhibits a weak cross peak to the heme 1CH<sub>3</sub> (Figure 4D). It is noted that the peptide NH for His I (207) (Figure 4C) resonates well to the low-field of the overwhelming majority of the residues, indicating it participates in a relatively strong H-bond.(29,30,33,43,44)

With a confirmed conserved molecular structure for residues Phe11-Phe192 for *Nm*HO<sup>A</sup>-PH-CN in solution(30) relative to that in crystal structures,(20,21) this His *I* has been concluded to arise from the C-terminal fragment His207-Arg208-His209 found "missing" in the crystal structures. The 8CH<sub>3</sub> cross peaks to the ring of Phe123 (Figure 4H) are stronger than predicted by the crystal structure, but can be accounted for by a small rotation of the Phe123 side chain, as discussed previously.(30) Comparison to the same spectral window for the 8CH<sub>3</sub> peak of *Nm*HO<sup>X</sup>-PH-CN demonstrates (particularly clearly observed in the NOESY 8CH<sub>3</sub> slices, Figures 4A and 4A') that both the His *I* ring and its backbone (not shown) NOESY cross peaks are completely lost, with only the 8CH<sub>3</sub>/Phe123 ring contact remaining (Figure 4H'). Several other cross peaks to 8CH<sub>3</sub> in the upfield aliphatic window (Figures 4A, 4B), which for *Nm*HO<sup>A</sup>-PH-CN have been attributed to Arg208 side chain protons, are similarly absent in the 'X' complex (Figure 4A').

The heme hyperfine shifts of the low-spin  $CN^-$  complex are perturbed by the 'A'—'X' conversion (Table 1), but not in any pattern consistent with rotation of either the heme or axial His.(35) Rather, the perturbation appears to manifest itself more in the pyrrole C/D portion of the heme. The local nature of the perturbation in the 'A'—'X' conversion is dramatically evidenced in the high-spin complex (compare Figures 2A and 2C), where only the 8CH<sub>3</sub> peak exhibits a detectably different environment in the two species. (All other resolved resonances exhibit essentially identical shifts in the 'A' and 'X' complexes). The dipolar shifted residues

in both NmHO-PH-CN and NmHO-PH-H<sub>2</sub>O, with the exception of the distal Leu119 and the proximal Asp24 in the former, and Asp24 in the latter (see below), exhibit essentially indistinguishable shifts and NOESY cross peak patterns in the 'A' and 'X' complexes (Table 1), indicating a highly conserved structure of the heme pocket, except at the solvent exposed pyrrole D.

Thus the most dramatic structural differences between the 'A' and 'X' NmHO-PH-CN species is the *complete loss of the 8CH<sub>3</sub> interaction with the C-terminal residue* His I (207)/Arg208 in the 'A' $\rightarrow$ 'X' conversion. The loss of this interaction with the C-terminus is the source of the sole perturbation of the 8CH<sub>3</sub> chemical shift in the high-spin complex 'A' $\rightarrow$ 'X' conversion (Figures 2A-2C).

# C-terminal cleavage in NmHOX

Identical mass spectra were detected for  $Nm{\rm HO^A}$  whether the apo- or substrate complexes were employed (not shown), confirming denaturation of the complex in the matrix. The predicted molecular mass of Met1-His209  $Nm{\rm HO}$  is 23,590 daltons. The  $[Nm{\rm HO^A}+{\rm H}]^{+1}$  ( $[Nm{\rm HO^A}+2{\rm H}]^{+2}$ ) peak in the MALDI-TOF mass spectrum of "native" or  $Nm{\rm HO^A}$  is observed at 23,454±13 (11,728±5) daltons (Figure 5A), using horse apo-Mb ( $M_r$  16,952) as internal standard, which reflects a 135±13 dalton difference (mass reduction) of neutral  $Nm{\rm HO^A}$  relative to that calculated for neutral Met1-His209. This difference is equally consistent with a missing Met1 ( $M_r$  131 daltons) or His209 ( $M_r$  137 daltons). N-terminal sequencing of  $Nm{\rm HO^A}$  reveals a homogeneous Ser-Glu-Thr-Glu-Asp-Glu-Leu-Thr-Phe, which uniquely identifies Ser2-Phe11 of the  $Nm{\rm HO}$  sequence and demonstrates that Met1 is cleaved during the processing of the enzyme in E.~coli. Hence the isolated enzyme (species 'A' or  $Nm{\rm HO^A}$ ) unequivocally consists of Ser2-His209 (with calculated neutral  $M_r$  = 23,459 daltons).

Mass spectrometry of ~10:1 and ~1:10 mixtures of  $NmHO^A$  and  $NmHO^X$  (as determined by  $^1H$  NMR in the cyanide complex) reveals a decreasing intensity for the peak centered at 23,450±15 daltons (labeled  $[NmHO^A+H]^+$ ) as shown in Figures 5B and 5C, respectively, which reflects a mass indistinguishable from that identified for pure  $NmHO^A$  in Figure 5A, and a new peak labeled  $[NmHO^X+H]^{+1}$ , with m/z 23,166±6 daltons, which reflects a reduction of neutral molecular mass relative to that calculated for Ser2-His209  $NmHO^A$  by 287±13 daltons. Nterminal sequencing of the 'A':'X' mixture again indicates a dominant (>90%) component with sequence identical to that obtained for pure  $NmHO^A$ , dictating that the mass reduction in 'X' relative to 'A' occurs at the C-terminus. The calculated  $M_T$  for Ser2-Pro206, Ser2-His207, and Ser2-Arg208 are 22,026, 23,163 and 23,322 daltons, respectively. Only the mass of Ser2-His207, 23,163 daltons, is consistent with the observed value of 23,166±6 daltons (neutral mass), dictating the species 'X', or  $NmHO^X$ , corresponds to Ser2-His207, which is equivalent to WT or species "A" with Arg208 and His209 deleted. Only the 23,450±15 and 23,166±6 dalton peaks are detected at intermediate degrees of  $A \rightarrow X$  conversion (not shown), suggesting that the Arg208His209 is cleaved as a dipeptide.

### **Assignment of His rings**

Long mixing time (40 ms) TOCSY spectra for primarily the  $NmHO^A$ -PH-CN complex in  $^2H_2O$  reveal the cross peaks between the ring  $C_\delta H$  and  $C_\epsilon H$  for 10 His, (not shown; see Supporting Information). With previous identification(30) of the strongly relaxed axial His23 ring (30), this locates all eleven of the His rings in native  $NmHO^A$ . Previous 2D NOESY contacts to the  $C_dHs$ , together with the conserved molecular structure for residues Phe11-Phe192 in solution relative to that in the crystal, had definitively identified(30) eight of the His rings (His23, 53, 58, 127, 137, 141, 145, 152; chemical shifts provided in Supporting Information.(30) The three remaining TOCSY ring cross peaks, with chemical shifts included in Table 1 (His I and J) and Supporting Information (His K), are labeled His I (close to 8-

CH<sub>3</sub> in 'A' complex), His *J* and His *K* (which collectively must arise from His159, 207, and 209); none of these three His rings exhibit any NOESY cross peaks that aid in their assignment.

Conversion of 'A'→'X' results in a TOCSY spectrum that also detects 10 rings (not shown; see Supporting Information). Seven His rings (plus the axial His23) exhibit the same diagnostic NOESY cross peaks that allow their assignments as reported for the 'A' complex (30) (not shown); the ring proton chemical shifts for these seven His rings are essentially independent of the 'A'  $\rightarrow$  'X' conversion (see Supporting Information). The TOCSY cross peak for His I of the 'A' species is clearly lost (as in its TOCSY-detected HisI NHC<sub>a</sub>HC<sub>b</sub>H<sub>2</sub> backbone; not shown) in the 'X' species. Neither His M nor His N in NmHOX-PH-CN (Table 1), that collectively must arise from His159 and His209, exhibit any detectable NOESY cross peak to the ring to guide their identification. Based on the observation that the ring shifts for the other seven assigned His are completely conserved in 'A' and 'X', the same shifts for His K in 'A' and His M in 'X' argue for their assignment to His 159, which is relatively remote from both C-terminus and heme. Hence His N in 'X' must arise from His 207, and its lack of NOESY cross peak argues for an orientation towards the solvent, as is consistent with its shifts. Formation of 'X' is also accompanied by the appearance of a new His ring peak at 8.30/6.78 ppm. Ultrafiltration of the solution reduces the intensity of this His N ring peaks, supporting the origin of this ring as the cleaved His209. The absence of additional NOESY cross peaks does not allow the determination by 2D <sup>1</sup>H NMR alone whether His207 or His209 interact with the heme 8CH<sub>3</sub> in NmHO<sup>A</sup>-PH-CN. Modeling the C-terminal interaction with the heme, however, strongly favors assignment of His I (in contact with 8CH<sub>3</sub>) as His207 (see below).

Nonetheless, the His ring TOCSY spectra provide additional evidence for the loss of a His ring in the 'A' $\rightarrow$ 'X' conversion, and the combination of the NMR, mass spectrometry and N-terminal sequencing data, clearly demonstrate that "aging" native *Nm*HO leads to loss of the two C-terminal residues, Arg208His209, and the abolition of the C-terminus interaction with the substrate.

# Cyanide affinity in NmHOA and NmHOX

Our interest here is to determine the *ratio of their cyanide binding constants*. With  $K_{eq}{}^{i} = [NmHO^{i}-PH-CN]/[CN^{-}][NmHO^{i}-PH]$  for i = 'A' or 'X', we obtain:

$$K_{eq}^{A}/K_{eq}^{X} = [NmHO^{A}PHCN][NmHO^{X}PH]/[NmHO^{X}PHCN][NmHO^{A}PH]$$
(1)

The two ratios, [NmHO<sup>A</sup>-PH-CN]/[NmHO<sup>X</sup>-PH-CN, and [NmHO<sup>X</sup>-PH]/NmHO<sup>A</sup>-PH], in Eq. (1) are determined from the relative intensities of the heme methyl peaks for the low-spin (Figures 6A'-6F') and high-spin (Figures 6A-6F) complexes under conditions where both the 'A' and 'X' complexes are significantly populated. As shown in the Figure 6, the high-spin species  $8CH_3^A$  peak preferentially loses intensity upon  $CN^-$  addition (Figures 6A-6F), while the low-spin species  $3CH_3^A$  peak preferentially gains intensity relative to  $3CH_3^X$  (Figures 6A'-6F'), dictating a stronger  $CN^-$  binding in the 'A' than 'X' species. The quantitation of the intensities by simulation yields  $K_{eq}{}^A/K_{eq}{}^X = 1.7 \pm 0.2$ .

### NMR spectra for the des-Arg208His209 deletion mutant ΔC2-NmHO

The resolved portions of the  $\Delta$ C2-NmHO- $H_2$ O and  $\Delta$ C2-NmHO-PH-CN  $^1$ H NMR spectra are provided in Figures 2D and 3D, respectively. Comparison of these to the analogous NmHO $^X$ -PH- $H_2$ O and NmHO $^X$ -PH-CN spectra in Figures 2C and 3C, respectively, reveals them to be indistinguishable in both the high-spin and low-spin complexes. This confirms not only that Arg208His209 are cleaved in the "aged" NmHO $^X$ , but that this is the only perturbation in the "aging". 2D NOSY spectra similarly reveal indistinguishable shifts and dipolar connectivities in the low-spin derivative (not shown).

## Heme degradation bound to NmHOs with ascorbate

The UV-visible spectra of the PH complexes of WT NmHO-PH-H<sub>2</sub>O and the mutant  $\Delta$ C2-NmHO-PH closely resemble each other (Figure 7). NmHO<sup>X</sup>-PH-H<sub>2</sub>O exhibited some differences from those of the above two enzymes, in that the ratio of the absorption at 406 nm to 280 nm (2.8) was slightly smaller than that (3.3) of the heme complex of wild-type enzyme. This suggests that the either 'X' species used in the present study included a little apo-enzyme resulting from release of a little heme during the conversion of the 'A' species to the 'X' species or some aggregation causes light scattering.

The ascorbate-driven activity resulting in degradation of PH was monitored by UV-visible spectroscopy for the three complexes, WT NmHO-PH-H<sub>2</sub>O, NmHO<sup>X</sup>-PH-H<sub>2</sub>O and  $\Delta$ C2-NmHO-PH-H<sub>2</sub>O. The WT NmHO-PH-H<sub>2</sub>O complex (Figure 8A, spectrum a) was quantitatively converted to ferric biliverdin (spectrum b), as previously reported. (45) Yoshida and Kikuchi (46) found that rat HO-1 in the presence of ascorbate yields ferric biliverdin, which yields the iron-free biliverdin on the addition of desferrioxamine, a ferric ion chelator. Therefore, we conducted a similar esperiment in the presence of desferrioxamine. The heme degradation rate was not affected by desferrioxamine, but a spectrum recorded 25 min after the start of the reaction showed a new broad absorption in the red region (spectrum c), suggesting a partial conversion of ferric biliverdin to iron-free biliverdin.

Figure 8B shows that the spectral changes observed for the  $Nm\rm HO^X$ -PH-H<sub>2</sub>O complex with ascorbate. When incubated with ascorbate alone, PH of this speices was degraded at a rate, and with resulting spectrum, very similar to those of wild-type enzyme, indicating that the final product is ferric biliverdin. However, when the reaction with  $Nm\rm HO^X$ -PH-H<sub>2</sub>O was conducted in the presence of desferrioxamin, the intensity of the broad band observed in the red region after 25 min incubation increased intensity by a factor ~2 (spectrum c in Figure 8B) as compared to that for the WT complex wild-type enzyme. As shown in Figure 8C, the reactivities of  $\Delta$ C2- $Nm\rm HO$ -PH-H<sub>2</sub>O complex are essentially the same as those of the  $Nm\rm HO^X$ -PH-H<sub>2</sub>O species. The product biliverdin revealed exclusively  $\alpha$ -stereoselectivity (data not shown) for both  $Nm\rm HOX$  and  $\Delta$ C2- $Nm\rm HO$ , as reported for WT  $Nm\rm HO$ .

These results indicate that, while neither the rate of heme degradation nor the stereoselectivity are detectably perturbed upon truncating *Nm*HO at the C-terminal by two residues, the truncation does influence the facility with which the product ferric biliverdin is released from the enzyme.

### DISCUSSION

# The nature of the NmHO 'Aging"

The available NMR and mass spectrometry data on the  $in \, situ$  "aged" WT NmHO and the NMR data on the synthetic  $\Delta$ C2-NmHO mutant, where Arg208 and His209 are deleted, clearly show that the "spontaneous aging" of NmHO results in the cleavage of the two C-terminal residues that interact with the substrate pyrrole D in the WT NmHO-PH-CN complex. While the mechanism of this aging is not understood at this time, it does not appear to be the result of either simple oxidative damage or the action of adventitious proteases which could co-purify with NmHO, and requires additional work well outside the scope of this report. What is important is that this "aging" of the resting state complex is sufficiently rapid to potentially interfere with all spectroscopic and functional studies carried out on a period of more than a few hours. The available new NMR results allow us to propose an improved model for the C-terminal interaction with substrate in the WT NmHO-PH-H<sub>2</sub>O complex that can account for altered functional properties of the "aged" complex.

### Structural changes accompanying the C-terminal cleavage

The essentially indistinguishable 2D NOESY maps for  $NmHO^{X}$ -PH-CN and the mutant  $\Delta C2$ -NmHO-PH-CN indicates that NmHO<sup>X</sup> and  $\Delta$ C2-NmHO are identical, and that our structural conclusions derived in detail for NmHO<sup>X</sup>-PH-CN are equally valid for the truncation mutant. The sequence origin of His I, in contact with the 8CH<sub>3</sub>, is either His207 or 209, but its identity could not be established on the basis of the presently available NOESY contacts alone. However, the available constraints do allow some limited modeling of the C-terminal His207Arg208His209 fragment that argues strongly for His I being His 207. In addition to the obvious loss of the His207 and Arg208 interaction with pyrrole D of the substrate, the deletions result only in very minor chemical shift change for the remainder of the active site. The heme resonance of the low-spin NmHO-PH-CN complex exhibit some perturbation of chemical shifts in the 'A' -- 'X' conversion, but the pattern of shifts, large spin density at heme positions 2-, 3-, 6- and 7-, and smaller spin density at positions 1-, 4-, 5- and 8-, reflective of the orientation of the axial His relative to the heme, is conserved.(35) In general, the substituents on pyrrole C and D exhibit the largest fractional change in hyperfine shifts. The majority of the dipolar shifted residues in the active site display insignificant shift changes with the loss of the Cterminus (Table 1 and Supporting Information). Particularly noteworthy are completely conserved dipolar shift for the proximal residues Thr19-Val26, (with one exception, Asp24; see below) and key distal residues Cys113-Phe123 (with the exception of Leu119; see below), which dictate completely conserved magnetic axes in the 'A' and 'X' complexes. The two residues with the largest shift perturbations, the proximal side Asp24 and distal Leu119 (Table 1), are rationalized by their very close proximity to the heme contact with the C-terminus in the NmHO<sup>A</sup>-PH-CN complexes (see below).

For the high-spin NmHO-PH-H<sub>2</sub>O 'A' and 'X' complexes, only the 8CH<sub>3</sub> of the resolved resonances exhibits detectably different hyperfine shifts for the heme (Figure 3A and Supporting Information), consistent with the primary contact of the C-terminus with 8CH<sub>3</sub>. The only assigned protons that exhibits(42) detectable shift change in the 'A'—'X' transition in the high-spin complex are the proximal Asp24 C<sub>β</sub>Hs (C<sub>β1</sub>H 0.1 ppm difference between 'A' and 'X' complexes; see Supporting Information). 2D <sup>1</sup>H NMR NOESY maps of apoNmHO<sup>A</sup> and apoNmHO<sup>x</sup> (not shown) are indistinguishable upon cursory inspection. The detectable difference in <sup>1</sup>H hyperfine shift pattern of the 'A' and 'X' PH complexes in the low-spin cyanide-inhibited forms shows that this is the optimal derivative for detection and structural characterization. However, at this stage, the most readily accessible technique for identifying the presence of NMHO<sup>x</sup> in any preparation, even in very small samples, is mass spectrometry.

### A model for WT NmHO species 'A'

There are insufficient NMR data available, and likely inaccessibility by solely  $^{1}$ H NMR, to construct a quantitative molecular model for the C-terminus interaction with the heme pocket for the  $NmHO^{A}$ -PH-CN complex. Such a study would require minimally  $^{15}$ N, and likely both  $^{15}$ N and  $^{13}$ C, labeling of NmHO, and 3D NMR, and is well beyond the scope of the present report. The route to efficient isotope labeling of NmHO is under study. However, the presently determined data do provide sufficient constraints to generate a qualitative model that accounts for the present observations, suggests consequences for functional roles for this interaction, and provides a potential rationalization for the 'loss' of the C-terminus in the crystal structures. (20,21) The most important of the new NMR data is the location of the complete backbone of His 207 which interacts strongly with the 8CH<sub>3</sub> (and weakly with 1CH<sub>3</sub>) and the recent report on the high-spin  $NmHO^{A}$ -PH-H<sub>2</sub>O complex where the resolved Asp24 C $_{\beta}$ Hs to Pro206 NOESY cross peak predicted by the crystal structure could be detected.(42) The expected NOESY cross peaks between the assigned Asp24 C $_{\beta}$ Hs and Pro206 in the low-spin NmHO-PH-CN complex are completely lost in the very intense aliphatic region of the NOESY map.

(30) Thus the positions of Pro206 in the crystal structure appears conserved in solution for *Nm*HO-PH complexes.

Our qualitative model results from the following data and their implications. First, we note that the ring protons for resonances His I and J (collectively His207 and 209) exhibit only very weak temperature-dependent chemical shifts, indicative of very small  $d_{\rm dip}$ , which argues for both ring orientations directed away from, rather than toward, the heme. Hence, imidazole ring contacts to the heme pocket are very unlikely candidates for the interactions that stablize the C-terminus contact with the heme pocket. This necessarily leaves the Arg208 guanidyl group as the main 'anchor' to the heme pocket. Moreover, if the Pro206 position in the crystal is largely maintained in solution, His207 is restricted to heme pocket interactions solely on the *proximal side*, with Arg208 restricted to either peripheral or distal interactions with the heme pocket. An orientation of the Arg208 side chain towards the heme dictates an 'outward' orientation of the ring of His209.

The following NMR data argue for the His *I* peptide NH as serving as a robust H-bond donor to a strong H-bond acceptor in order to orient the C-terminus: a) moderate intensity NOESY (Figure 4A, 4B) cross peak between significantly upfield dipolar shifted  $C_{\beta}$ Hs (by variable temperature behavior) of His *I* and PH 8CH<sub>3</sub> (a weak His*I*  $C_{\delta}$ H-8CH<sub>3</sub> NOESY cross peak likely arises via a secondary effect 8CH<sub>3</sub>- $C_{\beta}$ H- $C_{\delta}$ H); b) only a very low intensity NOESY cross peak between the His *I*  $C_{\delta}$ Hs and PH 1CH<sub>3</sub> (Figure 4D); c) a substantial low-field bias for the His *I* peptide NH (Figure 4C) when compared to the majority of the other NHs in the complex, in spite of a predicted upfield dipolar shift for protons in this region of space (Table 1) and, d) His *I* (207) NH exhibits only moderate intensity loss upon saturating the solvent signal (not shown), indicating a very slow exchange rate for pH 7.0 indicative of significant dynamic stability (33, 47, 48) for the interaction between the C-terminus and the substrate.

The only realistic acceptor for the Arg208 guanidyl terminus is the carboxylate of the 7propionate on PH. For the His207 peptide NH, the only "free" strong acceptor is the Asp27 carboxylate side chain. Using the constraints of a strong Arg208 guanidyl-7-propionate carboxylate salt bridge and a His207 peptide NH to Asp27 carboxylate H-bonds, and moderate distance (~4Å) between 8CH<sub>3</sub> and both His207 C<sub>B</sub>Hs and Arg208 C<sub>B</sub>H (based on NOESY cross peaks), molecular dynamics and energy minimization with conserved geometry of Phe11-Pro206 resulted in a qualitative model consistent with the proposed constraints, albeit not at the ideal distances. Releasing the Pro206 restriction leads to insignificant movement of this residue (~0.5Å), but yielded "good" His207 peptide H-bond and Arg208 salt bridge distances of ~3 Å. A molecular model for this C-terminus interaction with the active site in NmHO<sup>A</sup>-PH-CN is displayed in Figure 9. No unique orientation for the His209 ring is obtained, but it is shown oriented away from the heme pocket, as predicted above. The cleavage of Arg208His209 to form NmHOX abolishes the major stabilizing interaction between the Cterminus and heme, the Arg208-7-propionate link. The predicted dipolar shifts for His209 are included in Table 1 and are qualitatively consistent with the temperature dependence of the  $C_{\beta}H$  chemical shifts.

The side chain perturbation of the Asp24  $C_{\beta}H$  shifts both in the high-spin (see Supporting Information) and low-spin complexes (Table 1) during the 'A'  $\rightarrow$  'X' conversion is consistent with the loss of the His207 peptide NH H-bond to a proximal helix carboxylate. The carboxylate of both Asp24 and Asp27 on the proximal helix are sufficiently close so as to expect a significant chemical shift perturbation of one of the side chain protons if a salt bridge is broken in the adjacent carboxylate. The Asp27 residue signals have not been assigned in the low-spin complex (they are under the intense aliphatic envelope),(30) and are too strongly relaxed to resolve in the high-spin complex.(42) It is noted that in other HOs (16, 18, 22) the carboxylate of the homolog to Asp27 serves as H-bond acceptor to the axial His ring  $N_{\delta}H$ . However, in

NmHO, the H-bond to the axial His is provided by Asp24,(16, 21) freeing Asp27 to interact with the C-terminus. The perturbation of the Leu119 shifts in the low-spin complex (Table 1) can be expected in the 'A' $\rightarrow$ 'X' conversion because the Leu119 interacts strongly with the 7-propionate whose H-bond with Arg208 is broken.

## Implications for function and crystal structures

The demonstrated contact between the C-terminus and the substrate argues for some functional role for this interaction. On the one hand, the loss of the C-terminal contact with the heme in the 'X' form leads to a modest factor  $1.7 \pm 0.2$  decrease in cyanide affinity. The structural comparison and conserved dipolar shifts of the 'A' and 'X' forms reveals that the orientation of the magnetic axes is quantitatively conserved in the 'A'  $\rightarrow$  'X' conversion, arguing against direct contact between the C-terminus and ligand. However, compensation of the negative 7-propionate carboxylate charge in the distal pocket by the positive Arg208 guanidyl group in the native complex would be expected to facilitate the binding of negative ions in the 'A' forms.

The specifics of heme degradation in either  $NmHO^X$ -PH-H<sub>2</sub>O or the mutant  $\Delta C2$ -NmHO-PH-H<sub>2</sub>O complexes is unchanged and maintains the unique  $\alpha$ -stereoselectivity from that in the WT  $NmHO^A$ -PH-H<sub>2</sub>O. Thus the C-terminal interaction does not appear to serve a role in the factors that stabilizes the ferric hydroperoxy intermediate or direct it toward the  $\alpha$ -meso position by sterically orienting the hydroperoxy ion and blocking the other three meso positions. Moreover, essentially the same ferric biliverdin complexes are found in the truncated derivative and WT. What is notable is the significantly increased formation of free  $\alpha$ -biliverdin in the presence of desferrioxamine upon deletion of the C-terminal Arg208His209 as either  $NmHO^X$  or  $\Delta C2$ -NmHO. Thus the C-terminal interactions appear to retard loss of product.

The product biliverdin of the HO reaction is generally toxic and the overall HO rate is very slow ( $\sim 0.03 \text{ s}^{-1}$ ) for all HOs.(9) In mammals, the biliverdin off-rate is enhanced  $\sim 50$  fold upon binding biliverdin reductase, BVR, in a transient 1:1 complex, where the "docking" site has been identified (14) as the region of HO with the solvent exposed pyrrole. The enzyme that further processes biliverdin in pathogenic bacteria has not yet been identified. The effect on the product biliverdin off-rate upon eliminating the C-terminus suggests that the partner enzyme that processes the  $\alpha$ -biliverdin may "extract" the C-terminus of NmHO upon "docking", thereby facilitating product release. A more quantitative description of the detailed interaction of the C-terminus with substrate is clearly necessary, and routes to isotope labeling and structural characterization of the NMR-addressable NmHO-PH-CN complex are in progress. However, preliminary data on the native NmHO cyanide-inhibited substrate complex indicate that the C-terminal interaction with substrate can be significantly modulated by modifying the pyrrole substutients on pyrrole A and/or B (Liu, Y; Ma, L; Zhang, X; Yoshida, T; Satterlee, JD; La Mar, GN, unpublished). Since conversion of PH to its intermediates, αhydroxy-PH, α-verdoheme and ferric-α-biliverdin modifies the heme periphery near the pyrrole A/B junction, it is likely that the C-terminal interaction will depend on the nature of the intermediate, and structural characterization of the PH complex may or may not be relevant to the interaction of NmHO-bound ferric- $\alpha$ -biliverdin.

Lastly, the relative ease with which the 'A' $\rightarrow$ 'X' "aging" takes place in the laboratory in the absence of strong field ligands for the substrate complexes, suggest the possibility that properties of NmHO have been measured and reported on samples that may contain a significant amount of the 'X' form. The findings that the C-terminal His207Arg208His209 are "missing", and attributed to disorder in the crystal structure(20,21) could also be interpreted by a structure that has a significant fraction of the 'X' form with the Arg208His209 cleaved and His oriented randomly toward the solvent. Mass spectral data on the NmHO samples used for the crystal structure would resolve this issue.

## **CONCLUSIONS**

Solution <sup>1</sup>H NMR spectroscopy and mass spectrometry show that the heme oxygenase from *N. meningitidis* spontaneously cleaves its two C-terminal residues, Arg208His209. Two of the three C-terminal residues, His207Arg208, interact with the substrate in the native enzyme in a manner that appears to stabilize the bound form of the product ferric-α-biliverdin. The cleavage occurs over a wide range of rates depending on the nature of the substrate and axial ligand and is not inhibited in the absence of O<sub>2</sub> or in the presence of protease inhibitor cocktail. The spontaneous reaction is sufficiently facile in the resting state substrate complex (half life ~24h at 25°C, pH 7.0) to require great care in physico-chemical characterization of *Nm*HO complexes that may be variably, to completely, converted into the "aged" derivative. The reported "loss" of the C-terminal fragment in the crystal structure may have its origin in degraded HO. Comparison of the "aged" HO with the mutant with the two C-terminal residues deleted indicates that the C-terminal cleavage is the only process involved in the "aging".

# **Supplementary Material**

Refer to Web version on PubMed Central for supplementary material.

### References

- 1. Zhu W, Willks A, Stojiljkovic I. Degradation of heme in gram-negative bacteria: the product of the hemO gene of *Neisseriae* is a heme oxygenase. J Bacteriol 2000;182:6783–6790. [PubMed: 11073924]
- 2. Wilks A, Schmitt MP. Expression and characterization of a heme oxygenase (HmuO) from *Corynebacterium diphtheriae*. J Biol Chem 1998;273:837–841. [PubMed: 9422739]
- 3. Ratliff M, Zhu M, Deshmukh R, Wilks A, Stojiljkovic I. Homologues of Neisserial Heme Oxygenase in Gram-Negative Bacteria: Degradation of Heme by the Product of the pigA Gene of *Pseudomonas aeruginosa*. J Bacteriol 2001;183:6394–6403. [PubMed: 11591684]
- 4. Yoshida T, Migita CT. Mechanism of heme degradation by heme oxygenase. J Inorg Biochem 2000;82:33–41. [PubMed: 11132636]
- 5. Wilks A. Heme Oxygenase: Evolution, Structure, and Mechanism. Antioxidants Redox Signal 2002;4:603–614.
- 6. Frankenberg-Dinkel N. Bacterial Heme Oxygenases. Antoxidants Redox Signal 2004;6:825-834.
- 7. Ishikawa K, Sato M, Ito M, Yoshida T. Importance of histidine residue 25 of rat heme oxygenase for its catalytic activity. Biochem Biophys Res Commun 1992;182:981–986. [PubMed: 1540195]
- 8. Wilks A, Demontellano PRO. Rat Liver Heme Oxygenase High Level Expression Of a Truncated Soluble Form and Nature Of the Meso-Hydroxylating Species. J Biol Chem 1993;268:22357–22362. [PubMed: 8226746]
- 9. Ortiz de Montellano, PR.; Auclair, K. The Porphryin Handbook. Kadish, KM.; Smith, KM.; Guilard, R., editors. Elsevier Science; San Diego, CA: 2003. p. 175-202.
- 10. Ortiz de Montellano PR. The mechanism of heme oxygenase. Curr Opin Chem Biol 2000;4:221–227. [PubMed: 10742194]
- 11. Ortiz de Montellano PR, Wilks A. Heme Oxygenase Structure and Mechanism. Adv Inorg Chem 2001;51:359–407.
- 12. Rivera M, Zeng Y. Heme Oxygenase, steering dioxygen activation toward heme hydroxylation. J Inorg Biochem 2005;99:337–354. [PubMed: 15598511]
- 13. Davydov RM, Yoshida T, Ikeda-Saito M, Hoffman BM. Hydroperoxy-Heme Oxygenase Generated by Cryoreduction Catalyzes the Formation of α*-meso*-Hydroxyheme as Detected by EPR and ENDOR. J Am Chem Soc 1999;121:10656–10657.
- Wang J, Ortiz de Montellano PR. The Binding Sites on Human Heme Oxygenase-1 for Cytochrome P450 Reductase and Biliverdin Reductase. J Biol Chem 2003;278:20069–20076. [PubMed: 12626517]

 Unno M, Matsui T, Chu GC, Coutoure M, Yoshida T, Rousseau DL, Olson JS, Ikeda-Saito M. Crystal Structure of the Dioxygen-bound Heme Oxygenase from *Corynebacterium diphtheriae*. J Biol Chem 2004;279:21055–21061. [PubMed: 14966119]

- 16. Schuller DJ, Wilks A, Ortiz de Montellano PR, Poulos TL. Crystal structure of human heme oxygenase-1. Nature Struct Biol 1999;6:860–867. [PubMed: 10467099]
- 17. Lad L, Wang J, Li H, Friedman J, Bhaskar B, Ortiz de Montellano PR, Poulos TL. Crystal Structures of the Ferric, Ferrous and Ferrous-NO Forms of the Asp140Ala Mutant of Human Heme Oxygenase-1: Catalytic Implications. J Mol Biol 2003;330:527–538. [PubMed: 12842469]
- 18. Sugishima M, Sakamoto H, Higashimoto Y, Omata Y, Hayashi S, Noguchi M, Fukuyama K. Crystal structure of rat heme oxygenase-1 in complex with heme bound to azide: Implication for regiospecific hydroxylation of heme at the α-meso carbon. J Biol Chem 2002:45086–45090. [PubMed: 12235152]
- Sugishima M, Sakamoto H, Noguchi M, Fukuyama K. Crystal Structures of CO-, CN-, and NO-Bound Forms of Rat Heme Oxygenase-1 (HO-1) in Complex with Heme: Structural Implications for Discrimination between CO and O2 in HO-1. Biochemistry 2003;42:9898–9905. [PubMed: 12924938]
- 20. Schuller DJ, Zhu W, Stojiljkovic I, Wilks A, Poulos TL. Crystal structure of heme oxygenase from the Gram-negative pathogen *Neisseria meningitidis* and a comparison with mammalian heme oxygeanse-1. Biochemistry 2001;40:11552–11558. [PubMed: 11560504]
- 21. Friedman JM, Lad L, Deshmukh R, Li HY, Wilks A, Poulos TL. Crystal structures of the NO- and CO-bound heme oxygenase from *Neisseriae meningitidis* Implications for O2 activation. J Biol Chem 2003;278:34654–34659. [PubMed: 12819228]
- 22. Hirotsu S, Chu GC, Unno M, Lee DS, Yoshida T, Park SY, Shiro Y, Ikeda-Saito M. The Crystal Structures of the Ferric and Ferrous Forms of the Heme Complex of HmuO, a Heme Oxygenase of *Corynebacterium diphtheriae*. J Biol Chem 2004;279:11937–11947. [PubMed: 14645223]
- 23. Friedman J, Lad L, Li H, Wilks A, Poulos TL. Structural Basis for Novel δ-Regioselective Heme Oxygenation in the Opportunistic Pathogen *Pseudomonas aeruginosa*. Biochemistry 2004;43:5239–5245. [PubMed: 15122889]
- 24. Sugishima M, Migita CT, Zhang X, Yoshida T, Fukuyama K. Crystal structure of heme oxygenase-1 from cyanobacterium *Synechocystis* sp. PCC 6803 in complex with heme. Eur J Biochem 2004;271:4517–4525. [PubMed: 15560792]
- 25. Koenigs Lightning L, Huang H-W, Moënne-Loccoz P, Loehr TM, Schuller DJ, Poulos TL, Ortiz de Montellano PR. Disruption of an active site hydrogen bond converts human heme oxygenase-1 into a peroxidase. J Biol Chem 2001;276:10612–10619. [PubMed: 11121422]
- 26. Caignan GA, Deshmukh R, Wilks A, Zeng Y, Huang H-W, Moenne-Loccoz P, Bunce RA, Eastman MA, Rivera M. Oxidation of heme to β- and δ-biliverdin by *Pseudomonas aeruginosa* Heme Oxygenase as a Consequence of an Unusual Seating of the Heme. J Am Chem Soc 2002;124:14879–14892. [PubMed: 12475329]
- 27. Hernández G, Wilks A, Paolesse R, Smith KM, Ortiz de Montellano PR, La Mar GN. Proton NMR Investigation of Substrate-bound Heme Oxygenase: Evidence for Electronic and Steric Contributions to Stereoselective Heme Cleavage. Biochemistry 1994;33:6631–6641. [PubMed: 8204600]
- 28. Gorst CM, Wilks A, Yeh DC, Ortiz de Montellano PR, La Mar GN. Solution <sup>1</sup>H NMR investigation of the molecular and electronic structure of the active site of substrate-bound human heme oxygenase: the nature of the distal hydrogen bond donor to bound ligands. J Am Chem Soc 1998;120:8875–8884.
- 29. Li Y, Syvitski RT, Chu GC, Ikeda-Saito M, La Mar GN. Solution <sup>1</sup>H NMR investigation of the active site molecular and electronic structures of the substrate-bound, cyanide-inhibited bacterial heme oxygenase from *C. diphtheriae*. J Biol Chem 2003;279:6651–6663. [PubMed: 12480929]
- 30. Liu Y, Zhang X, Yoshida T, La Mar GN. <sup>1</sup>H NMR characterization of the solution active site structure of substrate-bound, cyanide-inhibited heme oxygenase from Neisseria meningitidis; Comparison to crystal structures. Biochemistry 2004;43:10112–10126. [PubMed: 15287739]
- 31. Zeng Y, Deshmukh R, Caignan GA, Bunce RA, Rivera M, Wilks A. Mixed Regioselectivity in the Arg-177 Mutants of *Corynebacterium diphtheriae* Heme Oxygenase as a Consequence of in-Plane Heme Disorder. Biochemistry 2004;43:5222–5238. [PubMed: 15122888]

32. Fujii H, Zhang X, Yoshida T. Essential Amino Acid Residues Controlling the Unique Regioselectivity of Heme Oxygenase in *Pseudomonas aeruginosa*. J Am Chem Soc 2004;126

- 33. Li Y, Syvitski RT, Auclair K, Wilks A, Ortiz de Montellano PR, La Mar GN. Solution NMR characterization of an unusual distal H-bond network in the active site of the cyanide-inhibited, human heme oxygenase complex of the symmetric substrate, 2,4-dimethyldeuterohemin. J Biol Chem 2002;277:33018–33031. [PubMed: 12070167]
- 34. Syvitski RT, Li Y, Auclair K, Ortiz de Montellano PR, La Mar GN. <sup>1</sup>H NMR detection of immobilized water molecules within a strong hydrogen-bonding network in the distal side of substrate-bound human heme oxygenase. J Am Chem Soc 2002;124:14296–14297. [PubMed: 12452690]
- 35. La Mar, GN.; Satterlee, JD.; de Ropp, JS. The Porphyrins Handbook. Kadish, KM.; Smith, KM.; Guilard, R., editors. Academic Press; San Diego: 2000. p. 185-298.
- 36. Johnston PD, Figueroa N, Redfield AG. Real-time solvent exchange studies of the imino and amino protons of yeast phenylalanine transfer RNA by Fourier transform NMR. Proc Natl Acad Sci USA 1979;76:3130–3134. [PubMed: 386331]
- 37. Jeener J, Meier BH, Bachmann P, Ernst RR. Investigation of Exchange Processes by Two Dimensional NMR Spectroscopy. J Chem Phys 1979;71:4546–4553.
- 38. Piotto M, Sandek V, Sklenar V. Gradient-tailored excitation for single quantum NMR spectroscopy of aqueous solutions. J Biomol NMR 1992;2:661–666. [PubMed: 1490109]
- 39. Griesinger C, Otting G, Wüthrich K, Ernst RR. Clean TOCSY for <sup>1</sup>H Spin System Identification in Macromolecules. J Am Chem Soc 1988;110:7870–7872.
- 40. Bax A, Davis DG. Mlev-17-based two-dimensional homonuclear magnetization transfer spectroscopy. J Magn Reson 1985;65:355–360.
- 41. Zhang X, Fujii H, Matera M, Migita CT, Sun D, Sato M, Ikeda-Saito M, Yoshida T. Stereoselectivity of each of the three steps of the heme oxygenase reaction: hemin to *meso*-hydroxyhemin, *meso*-hydroxyhemin to verdoheme, and verdoheme to biliverdin. Biochemistry 2003;42:7418–7426. [PubMed: 12809497]
- 42. Liu Y, Zhang X, Yoshida T, La Mar GN. Solution <sup>1</sup>H NMR characterization of the distal H-bond network and the effective axial field in the resting-state, high-spin ferric, substrate-bound complex of heme oxygenase from *N. meningitidis*. J Am Chem Soc 2005;127:6409–6422. [PubMed: 15853349]
- 43. Wagner G, Pardi A, Wüthrich K. Hydrogen Bond Length and <sup>1</sup>H NMR Chemical Shifts in Proteins. J Am Chem Soc 1983;105:5948–5949.
- 44. Li Y, Syvitski RT, Auclair K, Ortiz de Montellano PR, La Mar GN. Solution <sup>1</sup>H, <sup>15</sup>N NMR spectroscopic characterization of substrate-bound cyanide-inhibited, human heme oxygenase: water occupation of the distal cavity. J Am Chem Soc 2003;125:13392–13403. [PubMed: 14583035]
- 45. Zhu W, Wilks A, Stojiljkovic I. Degradation of Heme in Gram-Negative Bacteria: the Product of the hemO Gene of *Neisseriae* Is a Heme Oxygenase. J Bacteriol 2000;182:6783–6790. [PubMed: 11073924]
- 46. Yoshida T, Kikuchi G. Features of the reaction of heme degradation catalyzed by the reconstituted microsomal heme oxygenase system. J Biol Chem 1978;253:4230–4236. [PubMed: 96116]
- 47. Li Y, Syvitski RT, Auclair K, Ortiz de Montellano PR, La Mar GN. 1H NMR Investigation of the Solution Structure of Substrate-free Human Heme Oxygenase: Comparison to the Cyanide-inhibited, Substrate-bound Complex. J Biol Chem 2003;279:10195–10205. [PubMed: 14660632]
- 48. Englander SW, Kallenbach NR. Hydrogen exchange and structural dynamics of proteins and nucleic acids. Quart Rev Biophys 1984;16:521–655.

#### **ABBREVIATIONS**

НО

heme oxygenase

**NmHO** 

Neisseria meningitidis heme oxygenase

 $\Delta C2-NmHO$ 

Neisseria meningitidis heme oxygenase with Arg208/His207 deleted

**PaHO** 

Pseudomonas aeruginosa heme oxygenase

DSS

2,2-dimethyl-2-silapentane-5-sulfonate

**NOESY** 

two-dimensional nuclear Overhauser spectroscopy

**TOCSY** 

two-dimensional total correlation spectroscopy

**ROESY** 

two-dimensional rotating frame nuclear Overhauser spectroscopy

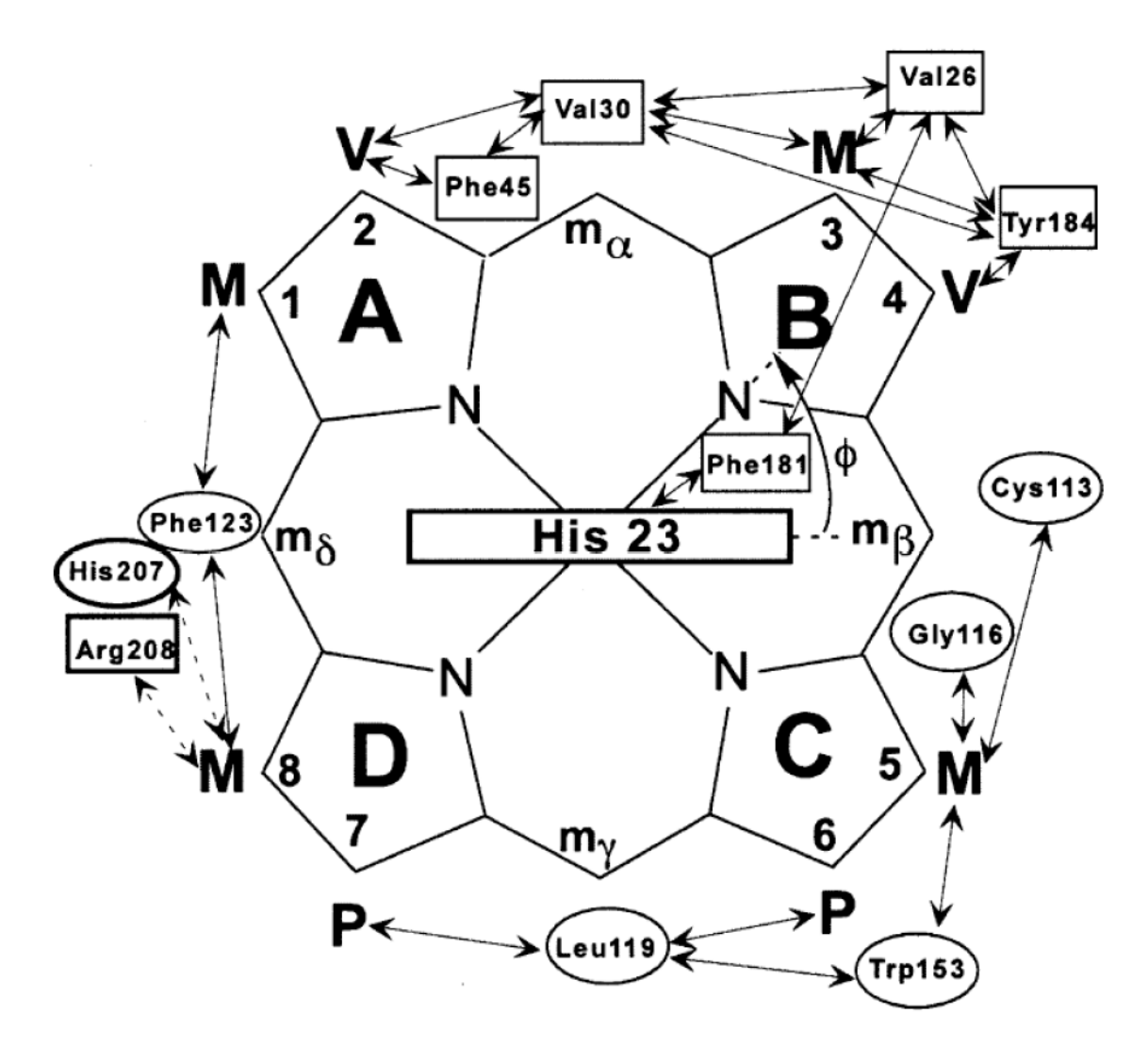


Figure 1. Structure of heme pocket of NmHO-PH-CN in solution as based on dipolar contacts between the protoheme substrate and a series of sequence specifically assigned heme pocket residues. Only seven key residues are shown, with rectangles and circles representing key proximal and distal residues, respectively. The two residues His I(207) (proximal) and Arg208 (distal) shown in bold, make contact with pyrrole D (dashed lines)only in the initially prepared or WT NmHO $^A$ -PH complex. Upon conversion to the NMHO $^X$ -PH complex, the pyrrole D contacts to His I(207) and Arg208 are lost.

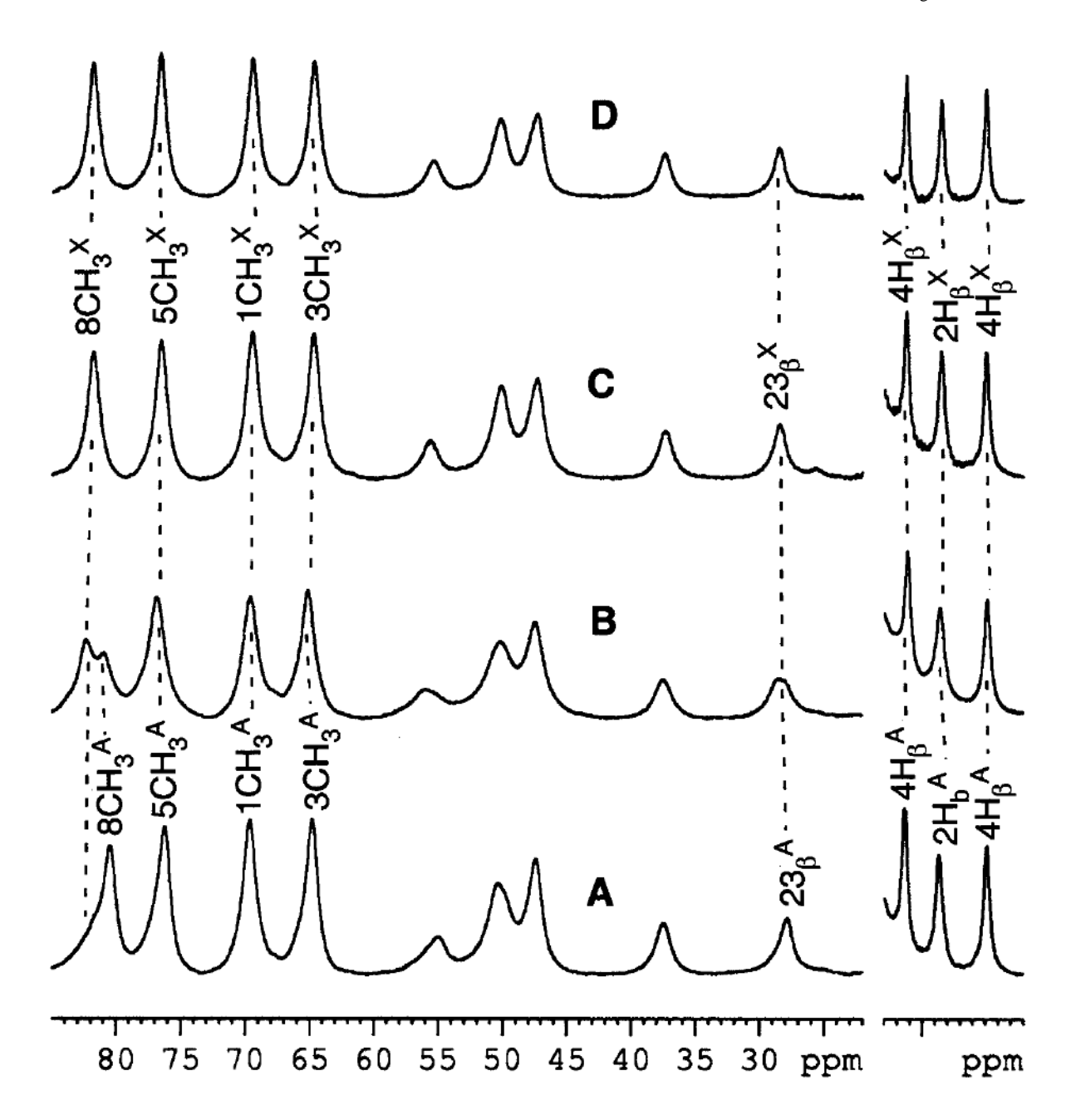
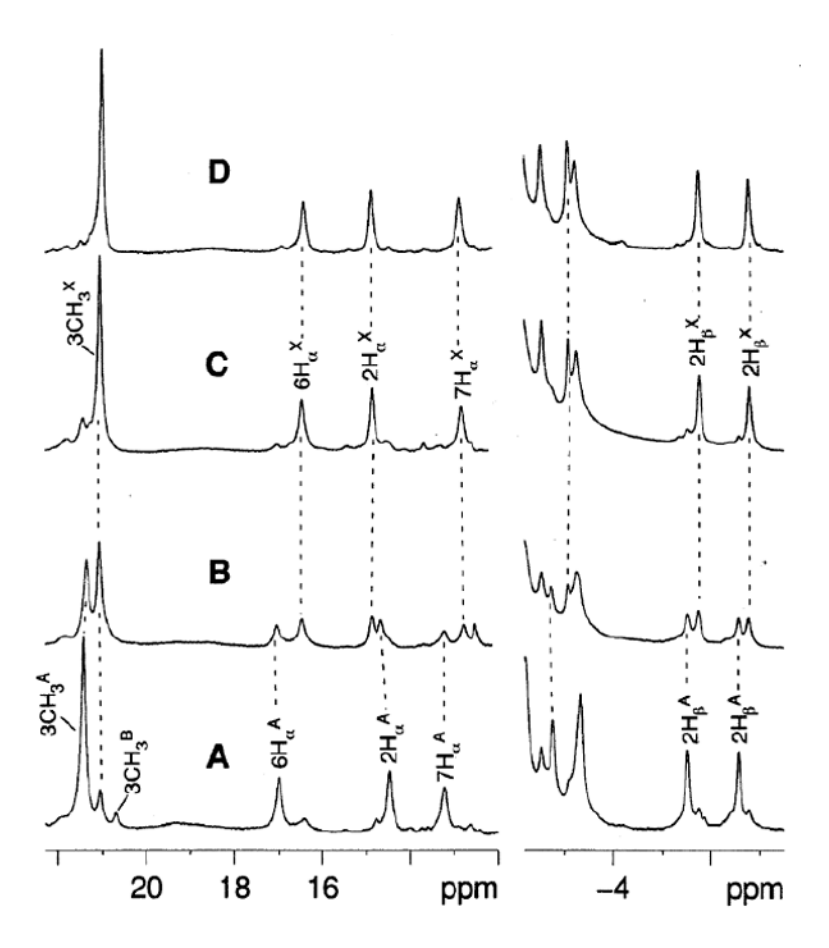


Figure 2. Resolved portions of the high-spin ferric NmHO-PH-H<sub>2</sub>O complexes in  $^2$ H<sub>2</sub>O, 100 mM in phospate, pH 7.0 at 25°C as: (**A**) the initially formed NmHO<sup>A</sup>-PH-H<sub>2</sub>O complex with assigned methyl and vinyl H<sub>β</sub> peaks; (**B**) a sample "aged" approximately 24 h at 25°C that consists of ~1:1 NmHO<sup>A</sup>-PH-H<sub>2</sub>O:NmHO<sup>X</sup>-PH-H<sub>2</sub>O, and (**C**) a sample "aged" for a week at 25°C which consists of predominantly NmHO<sup>X</sup>-PH-H<sub>2</sub>O; (**D**) illustrates the NMR spectrum for the deletion mutant  $\Delta$ C2-NmHO-PH-H<sub>2</sub>O (with Arg208/His209 deleted) which is indistinguishable from the "aged" NmHO<sup>X</sup>-PH-H<sub>2</sub>O complex in trace (**C**).



**Figure 3.** Resolved portions of the 600 MHz  $^1$ H NMR spectra, in  $^1$ H<sub>2</sub>O, 50 mM phosphate, pH 7.0 at 25°C, of: (**A**) low-spin, predominantly *Nm*HO<sup>A</sup>-PH-CN; (**B**) a ~1:1 mixture of *Nm*HO<sup>A</sup>-PH-CN and *Nm*HO<sup>X</sup>-PH-CN (population achieved upon 'aging' *Nm*HO-PH-H<sub>2</sub>O for ~40h at 25° C before adding CN<sup>-</sup>), and (**C**) primarily *Nm*HO<sup>X</sup>-PH-CN. Peaks are labeled by the Fischer notation for the heme (Figure 1), with the peaks for the alternate complexes, *Nm*HO<sup>A</sup>-PH-CN and *Nm*HO<sup>X</sup>-PH-CN, differentiated by a superscript A or X, respectively; (**D**) shows the  $^1$ H NMR spectrum for the truncation mutant ΔC2-*Nm*HO-PH-CN, where Arg208/His209 are deleted.

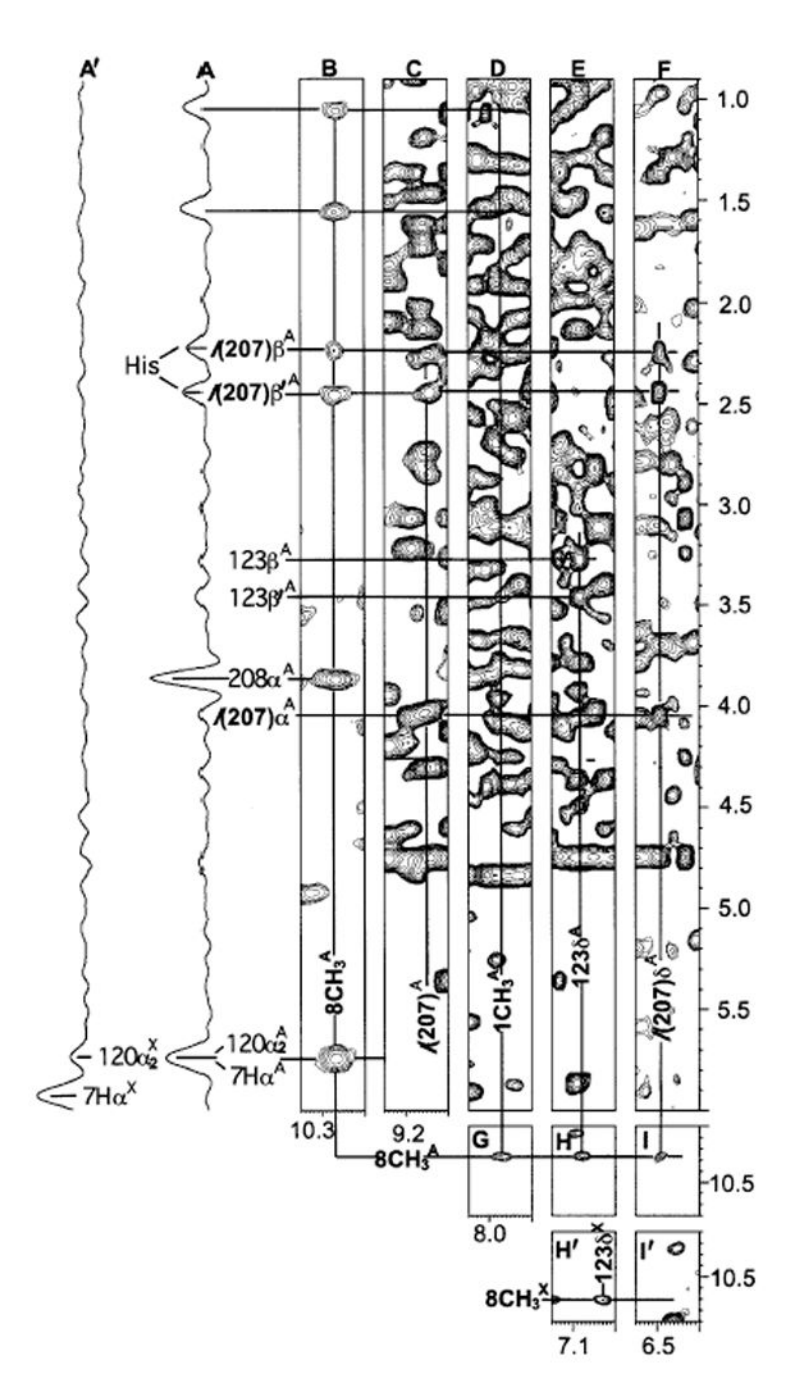


Figure 4. Portion of the 600 MHz  $^1$ H NOESY spectrum (**B-I, H', I'**) and NOESY slices through diagonal (**A**, **A'**) (mixing time 40 ms, repetition rate 1 s $^{-1}$ ); in  $^1$ H<sub>2</sub>O, 100 mM in phosphate, pH 7.0 at 25°C, of NmHO<sup>A</sup>-PH-CN (**A-I**) illustrating 8CH<sub>3</sub> NOESY cross peak to His *I* (207) C<sub>β</sub>Hs and Arg208 C<sub>α</sub>H (**A, B**), His *I*(207) C<sub>δ</sub>H (**F**) and Phe123 ring (**H**), 1CH<sub>3</sub> NOESY cross peak to His I(207) C<sub>β</sub>H (**D**), and His *I*(207) intra-backbone connection (**C**); and of NmHO<sup>X</sup>-PH-CN illustrating lack of either His *I*(207) or Arg208 C<sub>α</sub>H cross peak to 8CH<sub>3</sub> (**A'**), and His *I*(207) ring cross peak to 8-CH<sub>3</sub> (**I'**), but the retention of the Phe123 ring cross peak to 8-CH<sub>3</sub> (**H'**). The loss of the His *I*(207) and Arg208 cross peaks is particularly clear in the comparison of the slices through the 8CH<sub>3</sub> for the two complexes (**A**, **A'**).

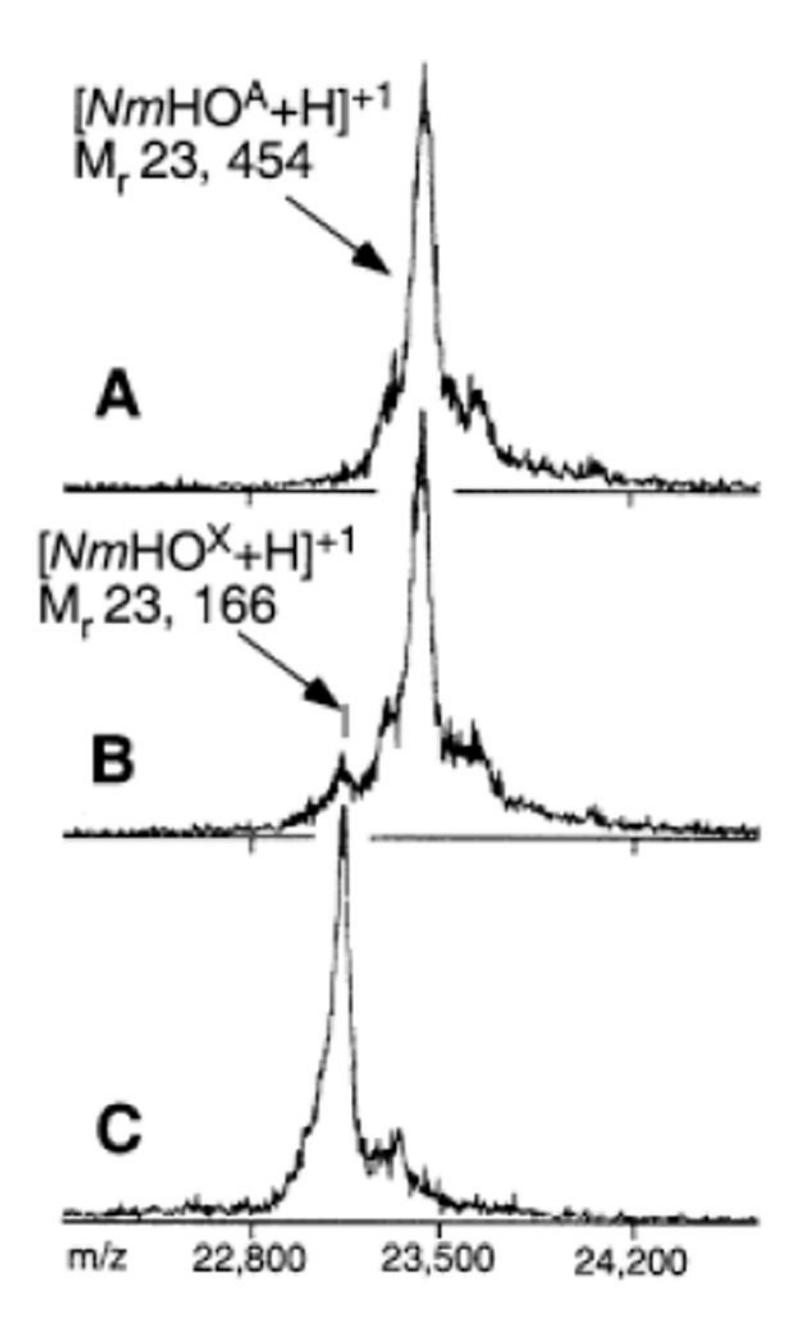


Figure 5. Portion of the MALDI-TOF mass spectra for  $M_r^+$ , obtained on the matrix consisting of sinapinicacid. Equine apoMb (Calc  $M_r = 16,924$ ) was used as internal calibrant. (A) Essentially pure (>95%)  $NmHO^A$ , which gives rise to  $[NmHO^A+H]^{+1} = 23,454\pm13$  daltons, and  $[NmHO^A+2H]^{+2} = 11,728\pm5$  daltons (not shown), indicative of a polypeptide  $135\pm15$  dalton smaller than that calculated for the sequence Met1-His209 ( $M_r = 23,590$ ), but consistent with  $NmHO^A$  as Ser2-His209. (B) A ~10:1  $NmHO^A:NmHO^X$  mixture, which yields a  $[NmHO^A+H]^{+1}$  peak of  $23,450\pm15$  and a weak new peak with  $M_r = 23,166\pm10$  assigned to NMHO<sup>X</sup>. (C) A in ~1:10  $NmHO^A = NmHO^X$  mixture (as determined by NMR) shows the new peak in (B), as now the major peak at  $26,168\pm10$ , and only as weak  $NmHO^A$  peak at  $23,459\pm15$  daltons. It is clear that the new peak with  $M_r \sim 26,166$  dalton represents the "aged"  $NmHO^X$  that corresponds to Ser2-His207 with Arg208His209 cleaved.

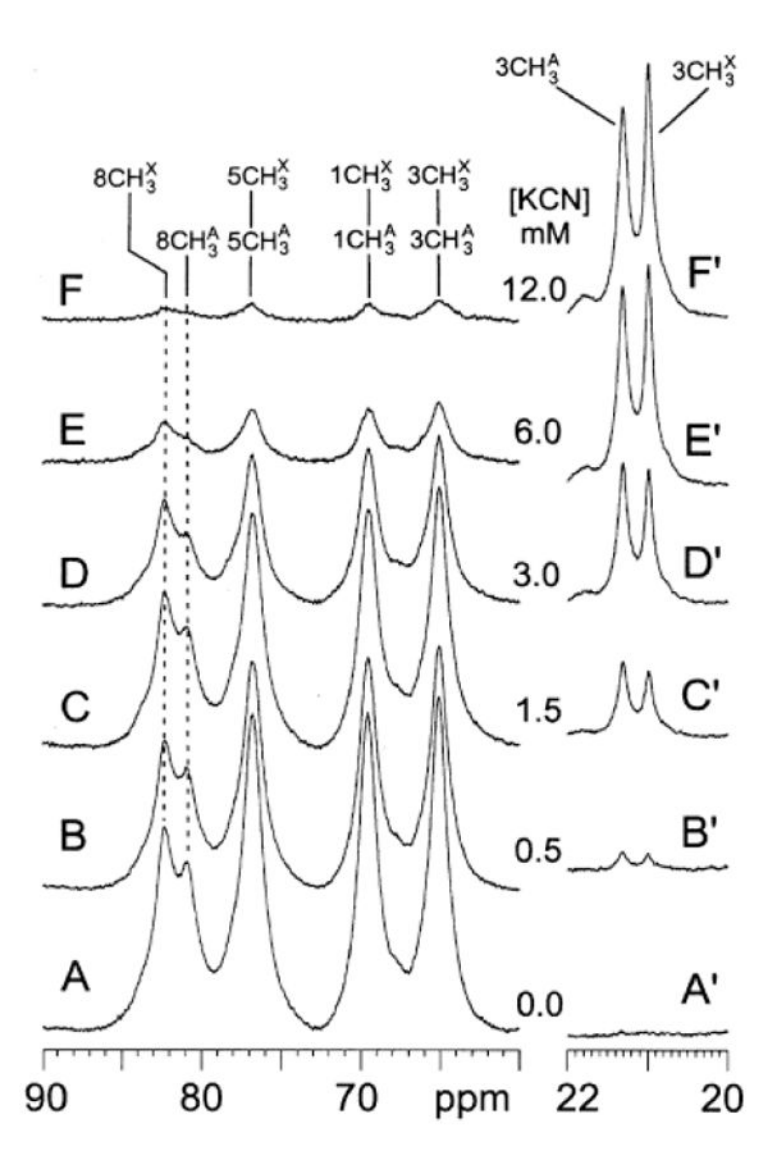
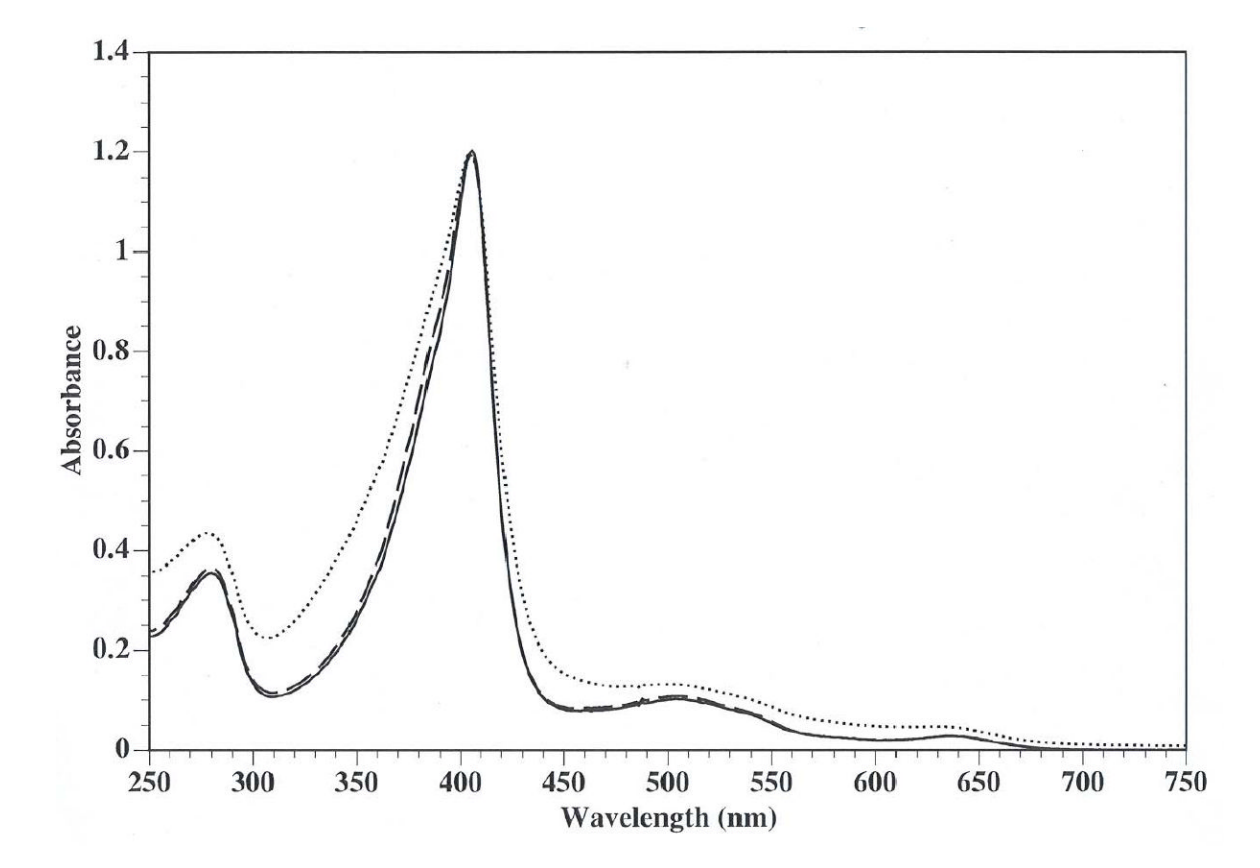


Figure 6. Low-field portion of the  ${}^{1}H$  NMR spectra of: (**A**) - (**F**) the high-spin NmHO-PH-H<sub>2</sub>O and (**A**')-(**F**') low-spin NmHO-PH-CN complexes for a 45:55 mixture of NmHO<sup>A</sup>-PH:NmHO<sup>X</sup>-PH, ~3 mM in NmHO, as a function of  $[CN^{-}]$ , in mM. Note preferential loss of  $8CH_{3}^{A}$  relative to  $8CH_{3}^{X}$  intensity upon increasing  $[CN^{-}]$  for the high-spin complex  $A \rightarrow F$ , and preferential increase of  $3CH_{3}^{A}$  relative to  $3CH_{3}^{X}$  intensity of low-spin complexes in  $A' \rightarrow F'$ .



**Figure 7.** Absorption spectra of the NmHO-PH-H<sub>2</sub>O complexes. Solid line, 10 mM of WT NmHO-PH-H<sub>2</sub>O complex; dotted line, about 10 mM of NmHO<sup>X</sup>-PH-H<sub>2</sub>O (an appropriate amount of the 'X' species was used so that the intensity of the Soret band is equal to that of wild-type complex); dashed line, 10 mM of  $\Delta$ C-NmHO-PH-H<sub>2</sub>O.

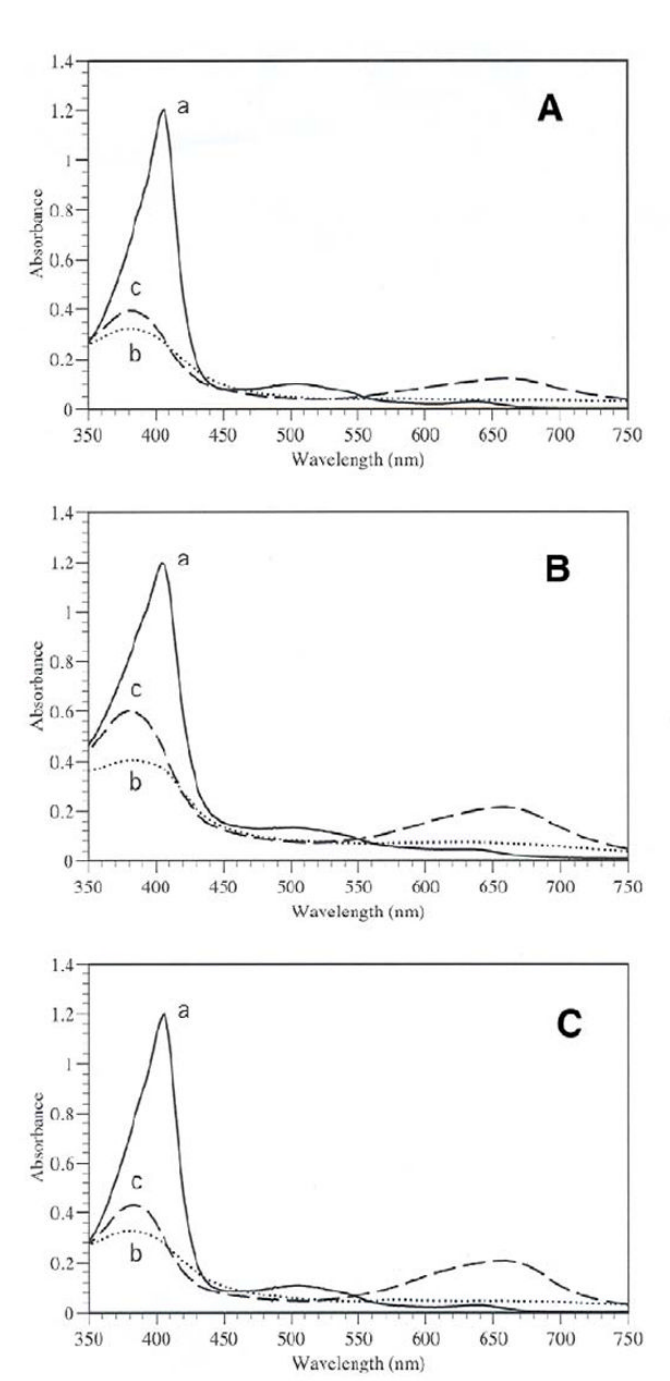


Figure 8. Ascorbate-driven degradation of PH bound to NmHOs in the absence or presence of desferrioxamine. Reaction mixture contained 10 mM NmHOs in 1.5 ml of 50 mM KPB (pH 7.4). After 3 min pre-incubation, the reaction was started by the addition of 15 ml of 1 M sodium ascorbate (final concentration, 10 mM). When desferrioxamine was added, a final concentration of 1 mM was used. (A) WT NmHO<sup>A</sup>; (B) the NmHO<sup>X</sup> species; (C)  $\Delta$ C2-NmHO. Spectrum **a** (solid line), before the start of the reaction; spectrum **b** (dotted line), 25 min after the start of the reaction without desferrioxamine; spectrum **c** (dashed line) 25 min after the start of the reaction with desferrioxamine.

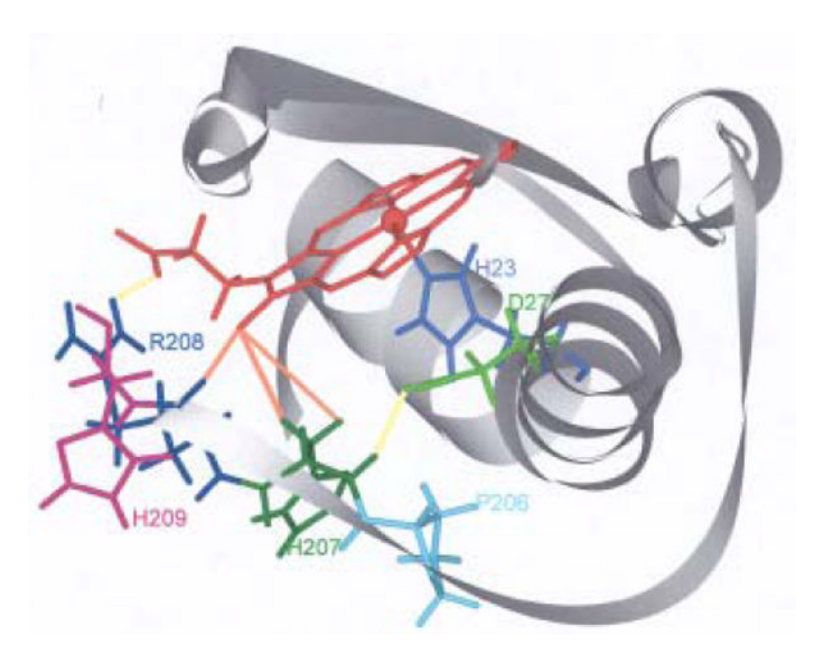


Figure 9. Molecular model of the C-terminus of  $NmHO^A$ -PH-CN with His207 (dark green) making a H-bond (yellow line) with the carboxylate of Asp27 (light green), and the guanidyl group of Arg208 (dark blue) making a salt-bridge (yellow line) with the carboxylate of the 7-propionate of PH (red). The crystallographic detected Pro206, the penultimate His209, and the axial His25 are shown as light blue, magenta and dark blue, respectively. Orange lines reflect important NOESY contacts of the PH 8-CH3 with the Arg208  $C_{\alpha}H$  and the two His207  $C_{\beta}Hs$ .

Scheme 1.

**Table 1**Chemical shifts for the heme and key heme pocket residues for the 'A' and 'X' forms of *Nm*HO-PH-CN

Residue	Proton	$Nm\mathrm{HO^{X}} ext{-}\mathrm{PH-CN}$ $\delta_{\mathrm{DSS}}(\mathrm{obs})^{a}$	NmHO <sup>A</sup> -PH-CN	
			$\delta_{ ext{DSS}}( ext{obs})^{ extbf{ extit{b}}}$	δ <sub>dip</sub> (calc) <sup>6</sup>
Heme	1-CH <sub>3</sub>	7.55	7.90	
	3-CH <sub>3</sub>	21.00	21.40	
	5-CH <sub>3</sub>	10.25	9.62	
	8-CH <sub>3</sub>	10.77	10.33	
	2 vinyl	14.79, -5.77, -6.79	14.48, -5.58, -6.62	
	4 vinyl	7.96, -3.09, -2.55	8.06, -3.38, -2.80	
	6-C <sub>α</sub> Hs	1.26, 16.40	1.14, 16.92	
	6-C <sub>β</sub> Hs	-0.88, -3.27	-1.02, -3.38	
	7-C <sub>α</sub> Hs	12.62, 5.92	13.06, 5.73	
	7-C <sub>β</sub> Hs	-1.23, -2.01	-1.10, -2.17	
	α-meso	-2.15	-2.21	
	β-meso	1.51	8.13	
	γ-meso	-1.64	-1.72	
Thr19	δ-meso NH	8.11	6.43 8.04	0.61
	$C_{\alpha}H$	5.53	5.52	0.96
	$C_{\beta}H$	5.77	5.75	1.12
	$C_{\gamma}H_3$	1.73	1.70	0.38
Γhr20	$C_{\gamma}^{\Pi_3}$ NH	8.43	8.37	1.15
	$C_{\alpha}H$	6.41	6.30	3.19
	$C_{\beta}H$	5.17	5.14	1.22
	C <sub>y</sub> H	2.30	2.27	1.96
Ala21	NΗ	9.37	9.36	1.37
11421	$C_{\alpha}H$	5.35	5.31	1.56
	$C_{\beta}H_3$	2.05	2.04	0.96
His23	NH	11.17	11.08	3.44
	$C_{\alpha}H$	7.30	7.37	6.01
	$C_{\beta 1}^{"}H$	11.51	11.56	
	$C_{\beta 2}^{P1}H$	10.88	10.75	
	$N_{\delta}^{\rho 2}H$	16.37	16.36	
	$C_{\delta}^{"}H$	18.4	19.2	
Asp24	NH	11.42	11.41	4.66
1	$C_{\alpha}H$	6.82	6.80	4.70
	$C_{\beta 1}^{"}H$	3.76	3.67	2.02
	$C_{\beta 2}^{P1}H$	4.30	4.30	2.37
Val26	NH	8.31	8.33	1.89
	$C_{\alpha}H$	2.79	2.80	-0.24
	$C_{\beta}^{m}H$	1.62	1.60	1.23
	$C_{\gamma 1}^{r}H_{3}$	-1.98	-1.96	-2.85
	$C_{\gamma 2}H_3$	-0.52	-0.5	0.18
Leu119	NH	10.62	10.54	2.20
	$C_{\alpha}H$	4.71	4.72	1.40
	$C_{\beta 1}H$	-1.31	-1.15	-0.82
	$C_{\beta 2}^{P}H$	-1.20	-0.95	-0.13
	C <sub>v</sub> H	-0.48	-0.40	
	$C'_{\delta 1}H_3$	-1.71	-1.69	-0.30
	$C_{\delta 2}^{01}H_3$	-0.70	-0.63	-2.54
Gly120	NH	13.5	13.6	8.49
	$C_{\alpha 2}H$	5.72	5.75	3.45
Ala121	NH	15.23	15.32	9.63
	$C_{\alpha}H$	8.43	8.52	8.77
	$C_{\beta}H_3$	5.51	5.44	5.06
Phe123	NH	8.81	8.83	1.50
	$C_{\alpha}H$	4.53	4.51	0.15
	$C_{\beta 1}H$	3.58	3.46	-0.54
	$C_{\beta 2}H$	3.37	3.27	-0.59
	CδHs	7.13	7.07	-0.81
	$C_{\varepsilon}Hs$	7.02	6.94	-0.09
	$C_{\zeta}H$	7.19	7.15	-0.56
Phe181	$C_{\delta}^{3}Hs$	7.22	7.25	0.16
	$C_{\varepsilon}Hs$	7.68	7.72	0.40
	$C_{\ell}H$	8.92	8.87	1.16
His I(207)	NH	-	9.15	-0.64

Residue	Proton	$Nm\mathrm{HO^X} ext{-}\mathrm{PH-CN}$ $\delta_{\mathrm{DSS}}(\mathrm{obs})^a$	$Nm\mathrm{HO}^\mathrm{A} ext{-}\mathrm{PH-CN}$	
			$\delta_{ ext{DSS}}( ext{obs})^{ extbf{ extit{b}}}$	$\delta_{ m dip}({ m calc})^{\it C}$
	C <sub>α</sub> H	-	3.84	-1.22
	$C_{\beta}H$	-	2.43	-0.54
	C <sub>B</sub> H'	-	2.22	-1.27
	$C_{\delta}^{P}H$	7.08	6.59	0.12
	C <sub>e</sub> H	7.93	7.68	0.22
rg208	$egin{array}{l} C_lpha H \\ C_eta H \\ C_eta H \\ C_lpha H \\ C_lpha H \\ C_lpha H \\ C_lpha H \end{array}$	d	3.84	-0.48
His $J(209)$	$C_{\delta}^{u}H$	d	7.92	-
	$C_{\epsilon}^{H}$		6.99	_

 $<sup>^</sup>a$ Chemical shifts in ppm, referenced to DSS via the solvent signal, in  $^1$ H2O, 100 mM in phosphate, pH 7.0 at 25°C.

 $<sup>^</sup>b$ Chemical shifts in ppm, referenced to DSS via the solvent signal, in  $^1$ H2O, 100 mM in phosphate, pH 7.0 at 25°C, as reported by Liu et al (30).

<sup>&</sup>lt;sup>c</sup>Calculated dipolar shift, in ppm, for NmHOA-PH-CN, as reported by Liu et al (30).